THESIS

THE VERTICAL DISTRIBUTION OF POLLUTANTS DURING EXPORT AND LONG RANGE TRANSPORT: A COMPARISON OF MODEL SIMULATIONS AND A-TRAIN OBSERVATIONS

Submitted By

Bonne Ford

Department of Atmospheric Science

In partial fulfillment of the requirements

For the Degree of Master of Science

Colorado State University

Fort Collins, CO

Spring 2011

Master's Committee:

Advisor: Colette Heald

Sonia Kreidenweis

Jennifer Peel

ABSTRACT

THE VERTICAL DISTRIBUTION OF POLLUTANTS DURING EXPORT AND LONG RANGE TRANSPORT: A COMPARISON OF MODEL SIMULATIONS AND A-TRAIN OBSERVATIONS

Due to increasing concern over the detrimental effects of pollution on visibility, human health, and agriculture, many countries have begun to set more stringent air quality regulations and to take measures to reduce local emissions. However, recent studies have also shown that long range transport (LRT) of pollution from upwind sources can make a non-negligible contribution to background concentrations and potentially inhibit a region's ability to meet air quality standards. Quantifying this contribution has become an important research initiative; however, a major hindrance in determining the impact of transported plumes on a receptor site lies in a lack of information on the vertical distribution of pollutants during export and transport from a source region. The vertical distribution can determine the efficiency of transport by way of dominant removal processes and wind strength, which will determine the final surface impact at a downwind site.

In this study, we integrate aerosol extinction and optical depth observations from the Cloud-Aerosol Lidar with Orthogonal Polarization (CALIOP), aerosol optical depth AOD from the Moderate-resolution Imaging Spectroradiometer (MODIS) along with

measurements of carbon monoxide (CO) from the Tropospheric Emission Spectrometer (TES) with simulations of species concentrations from a global chemical transport model (GEOS-Chem) to examine the differences in gas and aerosol phase transport in the Northern Hemisphere. The different vertical structures exhibited by gaseous and particulate phase pollution due to differing sources and sinks provide opportunities to evaluate the model representation of mechanisms that determine the vertical structure, and ultimately the impact of LRT downwind. While CALIOP has unprecedented vertical resolution, it, like TES, has a small footprint and wide distance between scans, with no cross-track scanning. Therefore, comparisons with these satellite observations are particularly susceptible to model transport errors, especially on short time scales. We choose to minimize the effect of these sampling biases by examining LRT on a seasonal timescale.

From seasonal comparisons, it is evident that pollutants are exported from their source regions throughout the year; however, the most efficient transport of CO and aerosols happens in spring due to more efficient mechanisms for lofting. We also investigate the strong regional dependence, where pollutants experience higher lofting over the eastern coastal regions of Asia and North America compared to Europe. In GEOS-Chem, pollutants that are lofted are more efficiently transported, while pollutants in the boundary layer are quickly removed. For CO, GEOS-Chem shows no particular bias compared to observations in the vertical distribution; however, these CO observations have limited vertical sensitivity. Aerosol extinction observations from

CALIOP have increased vertical sensitivity and suggest that GEOS-Chem shows a high bias in source regions such as East Asia and over Europe, and a conversely low bias in outflow regions.

ACKNOWLEDGEMENTS

I thank my advisor, Colette Heald, for the continual help and guidance she provided throughout my master's degree program. I also thank my committee members, Sonia Kreidenweis and Jennifer Peel, for their help and insight with this work.

I also want to express my gratitude to Ball Aerospace for funding my master's graduate work and especially, James Leitch, Shelley Petroy, and Carl Weimer, who all took special interest in my research project.

Finally, I am grateful for the encouragement of my family and friends; and in particular, for the advice and humor of Ezra Levin and David Ridley throughout this process.

TABLE OF CONTENTS

LIST OF FIGURES

1 Introduction

The detrimental effects of atmospheric pollution on human health, agriculture, and visibility have motivated many countries to set stringent air quality regulations (Air Quality Standards Regulations 2010; 40 C.F.R. 50, 2010). Although local emission sources are the main cause of air quality degradation, episodic long range transport (LRT) can also contribute to elevated pollutant concentrations (Li et al., 2002; Parrish et al., 2009). It has therefore become necessary to view pollution on a more global scale and consider the pathways and mechanisms that determine the impact of long range transport in different regions. In particular, in this study our objective is to investigate the vertical structure of pollution during long range transport, and how this dictates air quality impacts downwind.

Improving air quality has become a major concern for many countries due to the widespread realization that air quality degradation poses a serious threat to human health (Bell et al., 2004; Pope and Dockery, 2006). For the United States, the Environmental Protection Agency (EPA) sets National Ambient Air Quality Standards (NAAQS) for six criteria pollutants which are harmful to human health and the environment: carbon monoxide (CO), lead (Pb), nitrogen dioxide (NO_2), ozone (O_3), particulate matter (PM), and sulfur dioxide (SO_2) (www.epa.gov). Studies have shown that exposure to particulate matter (PM) is associated with increased risk of lung cancer and cardiopulmonary mortality (Pope et al., 2002; 2004) and that exposure to ozone is associated with premature mortality (Bell et al., 2005), aggravated asthma (Gent et al.,

2003; Lin et al., 2008) and other respiratory diseases (Burnett et al., 1997). Additionally, studies have shown that the positive association between PM or ozone exposure and elevated rates of premature mortality is evident even at concentrations below current regulatory levels (Pope, 2000; Daniels et al., 2000; Bell et al., 2006). For particulate matter, this suggests that, regardless of local background concentrations, any increase in exposure, such as from LRT, leads to increased premature mortality (Liu at al., 2009). While countries have made efforts to lessen exposure and improve air quality by setting stricter regulations, LRT could additionally make it more difficult to meet these air quality standards (Schultz and Bey, 2004). For example, Li et al. (2002) use model simulations to suggest that 20% of the ozone violations in Europe during the summer of 2007 would not have occurred in the absence of North American anthropogenic emissions.

Although there is evidence for the long range transport of many atmospheric constituents, most research has focused on the regulated species such as PM, ozone, and its precursors. Additionally, while the term "long range transport" can be used on scales of tens of kilometers, we focus here on hemispheric scale transport between continents. There have been several studies addressing the impact of transatlantic transport of ozone and related species from the eastern US to Europe (Guerova et al., 2006; Derwent et al., 2004), transpacific transport of Asian dust and pollution on air quality in the western US (Akimoto, 2003; Reidmiller et al., 2008; Heald et al., 2006; Jaffe, 1999), export of anthropogenic pollutants from Europe to Africa, Asia, and the Arctic (Duncan and Bey, 2004; Quinn et al., 2007) and dust from Africa to South America and the Caribbean (Prospero, 1981; Ansmann, 2009). In this study we choose to focus on the Northern

Hemisphere because it has more landmass with higher anthropogenic emissions and the majority of the world's population, making LRT a more frequent and potent problem than in the Southern Hemisphere. Specifically, we examine export and transport in the mid-latitudes out of three main regions: Asia, Europe, and North America.

The effectiveness of long range transport of pollutants from these source regions to downwind receptor sites is determined by several factors: the initial amount emitted, the lifetime of the species against transformation and removal, the contribution from en-route production, the transport pathway, and transport efficiency (how quickly a pollutant is transported with respect to its lifetime). Transport can occur at low altitudes through boundary layer ventilation or advection with the mean winds, but these processes generally take place on timescales of days to weeks, and therefore are inefficient for chemical species with shorter lifetimes. However, while ozone and PM have lifetimes on timescales of only hours to days in the boundary layer before removal or chemical transformation, if they are lofted into the colder free troposphere, their lifetimes can be extended (Keating and Zuber, 2007). Furthermore, since winds generally strengthen with height, they can be transported more rapidly. Therefore, for more efficient transport, pollutants must first be vertically lofted out of the boundary layer and into the upper troposphere through strong convection, warm conveyor belts, turbulent mixing, or orographic lifting. Several studies have also noted that while many particles are removed near the source during lofting, production can occur en route through gas-to-particle phase conversion (Brock et al., 2004; Dunlea et al., 2009).

Given the efficiency of transport in the free troposphere, many LRT events have been detected at elevated sites such as the Mount Bachelor Observatory (Reidmilller et

al., 2009) or the PICO-NARE station on Pico mountain (Owen et al., 2006). Clean background air sampled at these sites also facilitates the identification of transported plumes. While transport is more efficient in the free troposphere; if plumes remain aloft, they might affect clouds or precipitation (Brock et al., 2004), free tropospheric chemistry or upper air visibility, but they will have no impact on lower altitude surface sites. Pollutants can descend with the aid of mountain circulations and subsidence associated with subtropical highs and cause surface air quality disturbances. The efficiency of the descending process would ultimately determine the magnitude of the disturbance or contribution to background concentrations. However, detecting an observable influence of LRT at the surface is complicated by local influences and the dilution of plumes during descent (Hudman et al., 2004; Heald et al., 2006).

Identification of LRT plumes is also complicated by the fact that long range transport often occurs over ocean basins or remote continental regions where observations are limited. Assessing LRT impacts has therefore relied on interpreting the observational record at a receptor region (e.g. Prospero, 1999; Jaffe et al., 1999) or at an island site located between source and receptor (Levy and Moxim, 1989; Perry et al., 1999) with little information on the processes that occurred during transport. Aircraft data from field campaigns have provided useful information about the vertical distribution and specific in-plume processing of pollutants, as aircraft are able to follow plume progression and sample the same plume multiple times, but like surface observations, these campaigns still suffer from spatial and/or temporal constraints (Hudman et al., 2004; Heald et al., 2004; Price et al., 2004; Singh et al., 2006; Fehsenfeld et al., 2006; Fuelberg et al., 2010). While satellite observations offer the possibility of continuous

global coverage, due to poor vertical resolution, satellites have been primarily used to track the spatial progression of plumes (Yu et al., 2008; Heald et al., 2004; 2006; Edwards et al., 2004). However, merely examining the spatial distribution of column totals provides an incomplete picture of the vertical distribution of pollutants during transport and restricts our understanding of how plumes progress. Ultimately, this lack of information on the vertical distribution makes it more difficult to translate these satellite observations into surface concentrations and determine the impact on air quality at downwind sites (Al-Saadi et al., 2005; van Donkelaar, 2010).

The implementation of improved satellite technology with heightened vertical resolution has therefore provided the opportunity to better examine the export and long range transport of pollutants. The CALIOP instrument, a space-based lidar, provides an unprecedented look at the vertical distribution of clouds and aerosols in the global atmosphere (Winker et al., 2010). Because carbon monoxide (CO) has strong absorption lines in the thermal infrared (IR) and solar shortwave IR, which are observable from space; by using calibrated measurements of CO radiance, instruments such as TES are able to retrieve vertical information on the distribution of CO (Deeter et al., 2004).

Several studies have already taken advantage of the vertical distribution of aerosols provided by CALIOP, but to primarily look at dust transport. Generosa et al. (2008) found that dust was exported in plumes off of western Africa that slowly descend as they traverse the Atlantic. In winter, this occurs in more shallow layers (under 4km), while in summertime, plumes can extend up to 6-8km. Yu et al. (2010) also looked at the vertical distribution of dust along with the total extinction due to aerosols in different source regions, similarly finding that high extinction values are found up to much higher

altitudes in the spring and summer than in the fall and winter. Additionally, aerosols from dust and biomass burning regions are generally lofted more than aerosols from industrial regions.

Differences in transport height according to source type region have also been noted for gas phase pollutants. For example, Liu et al. (2003) found in both aircraft data and model simulations that Asian biomass burning was transported in distinct elevated layers, while Asian anthropogenic CO could also be transported in the boundary layer. They also found that export can vary drastically by season, with a maximum in early spring and a minimum in summer, differing by a factor of 3-4. Liang et al. (2004) also examined the variations of Asian CO export and the impact on the North Pacific and western US and found that in spring that the Asian contribution to a Washington state coastal site could be up to 24ppb in summer and 44ppb in spring.

While observations have been used to identify LRT events, accurately attributing sources of surface pollutants at a receptor site can be difficult, especially when pollutants may have large background concentrations, high local emissions, or incoming plumes have been heavily diluted or undergone chemical transformation. For this reason, many studies have also relied on chemical transport models for source attribution and for assessing receptor responses to emissions changes (Fiore et al., 2009). By altering model emissions and comparing with surface networks, Park et al. (2004) and Chin et al. (2007) examined the contribution of local and transboundary pollution on surface concentrations. Using the GOCART model, Chin et al. estimated that on an annual average, long range transport of aerosols from combustion sources accounts for ~0.2 μgm^{-3} of the fine mass (which is 2-6% of the total fine mass) over the US and transport of

dust accounts for 0.5-0.8 μgm^{-3} (or 6-24% of the total) Park et al. (2004) found that transboundary pollution contributed more to the background concentrations of sulfate and nitrate than natural sources in the US and specifically, that transport from Asia accounts for ~30% of the background sulfate concentrations. Guerova et al. (2006) also conducted model sensitivity studies to determine the contribution from North America to summertime ozone concentrations over Europe, finding it to be 3-5ppb in the planetary boundary layer (PBL) and 10-13ppb in the middle to upper troposphere.

For this study, we use A-Train observations, including CALIOP aerosol extinction, Aqua MODIS aerosol optical depths (AOD) and TES retrievals of CO to study long range transport in the Northern Hemisphere. In particular, we use these observations to test the vertical representation of transport processes in the global chemical transport model GEOS-Chem. Carbon monoxide is used here as a contrast to aerosol, whose shorter lifetime and higher solubility suggest different transport pathways (Heald et al., 2006). Given the challenges of detecting near surface concentrations with satellites, we also incorporate data from ground based sites, specifically the IMPROVE aerosol monitoring network. We use the GEOS-Chem model to interpret these observations and to identify contributions due to differing sources and species.

2 Descriptions of Observation and Modeling Tools

2.1 Satellite Observations

2.1a CALIOP

The Cloud-Aerosol Lidar with Orthogonal Polarization (CALIOP) was launched aboard the Cloud-Aerosol Lidar and Infrared Pathfinder Satellite Observations (CALIPSO) satellite on April 28, 2006 as part of the A-Train constellation. CALIOP measures the backscatter intensity and the orthogonally polarized components of the backscatter signal at two wavelengths, 532nm and 1064nm (Winker, 2003). CALIPSO takes 16 days to repeat its orbit; and with a 30 m vertical resolution in the troposphere and a ~100 m footprint (officially 70m, but without hard edges), full global coverage for CALIPSO also takes approximately 16 days (Hunt et al., 2009).

For aerosol extinction data, we use the CALIPSO Lidar Level 2 Version 3.01 5-km Aerosol Profiles for December 2006 through November 2007 and filter the data using cloud aerosol distinction (CAD) scores, extinction uncertainty values, atmospheric volume descriptors, extinction quality control (QC) flags and total column optical depths. CAD scores are a numerical measure of the confidence of the algorithm classification of observed layers, with negative values used for aerosols and positive values for clouds (Liu et al., 2004). Therefore, we discard any observations with absolute values below 20, which is a more relaxed criterion than Yu et al. (2010) suggests, but allows for a greater sample volume. We also choose to use only clear sky columns by discarding any columns

with cloud optical depths greater than zero. Additionally, since CALIOP cannot make observations below thick aerosol layers, we omit any columns with aerosol optical depths greater than two, although this can, in rare circumstances, eliminate pollution events. Extinction uncertainty values and quality control flags are used to remove any observation where the extinction calculation failed or produced non-physical results. We make the approximation that all extinction observations with a corresponding atmospheric volume descriptor that indicates clear air have zero aerosol extinction. We chose to assign a value of zero rather than a value related to the detection limit because there is not one standard detection limit, but is instead dependent on assumed aerosol type. For the night (day) observations, this filtering eliminates ~17% (12%) of the extinction values and makes ~77% (84%) of the extinction values 0.

CALIPSO has an ascending equator crossing at 1330 local solar time (LST) and a descending node at 130 LST. While Kittaka et al. (2010) have shown that CALIOP AOD distributions derived from the earlier Level 2 Version 2.01 layer products are similar for day and night, for this work, except for comparison with MODIS, we choose to use the nighttime data because the signal-to-noise ratio (SNR) is greater during the night due to the lack of noise from background solar illumination (Hunt et al., 2009). We repeat the comparison of Kittaka et al. for the dataset used here and find similar results (Figure 2.1).

2.1b MODIS

The Moderate-resolution Imaging Spectroradiometer (MODIS) measures scattered radiances at 36 wavelengths and provides almost daily global coverage of AOD observations in the absence of clouds with a 500m resolution. Because removing the contribution of surface reflectance from the measured top of the atmosphere reflectance is

crucial for determining AOD, two different algorithms are used for AOD retrievals over the ocean and the land. Over the dark ocean, seven spectral channels are used and the

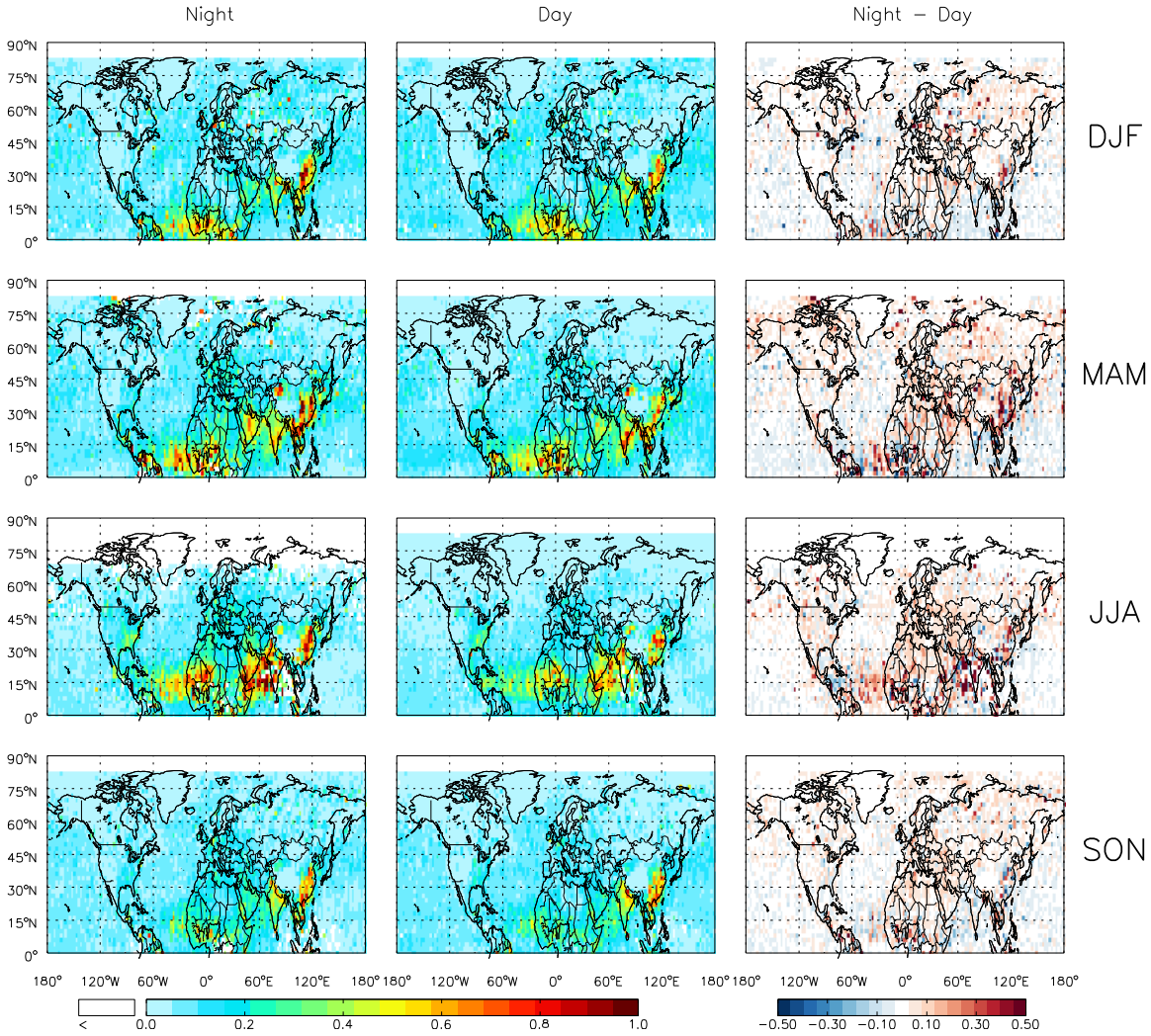

Figure 2.1: Seasonal averages of CALIOP AOD for December 2006-November 2007 (saturated out at 1.0) using night overpasses (column 1) and day overpasses (column 2), and the seasonal difference (column 3).

contribution from surface reflectance is easily removed. Over the varying land surface, only three channels are used and a surface reflectance has to be assumed. Although AOD is only retrieved over dark surfaces while cloudy or snow-covered pixels are masked out

(Kaufman et al., 1997), this use of an estimated surface reflectance has led to a high bias over land (Drury et al., 2008).

For this work, we use data from MODIS aboard the Aqua platform which flies in the A-Train constellation, one minute and fifteen second ahead of CALIPSO. Specifically, we use Collection 5, Level 3 daily files, which are on a 1º by 1º grid. We combine land and ocean optical depth retrievals, and filter the data to include only columns with cloud fractions below 0.8 and aerosol optical depths less than 1.5 (Zhang and Reid, 2006).

Kittaka et al. (2010) compared daytime AODs from MODIS and an earlier version of CALIOP retrievals for the period June 2006 to August 2008 and found that daytime CALIOP observations were generally biased high. We also compare seasonal average AODs from MODIS and CALIOP for 2007 (figure and further discussion in Chapter 5). Differences between the two can be partially explained by the known biases associated with each instrument, and further comparisons will be discussed in subsequent chapters.

2.1c TES

We use observations of CO from the Tropospheric Emission Spectrometer (TES), which is one of four instruments aboard the NASA Earth Observing System (EOS) Aura platform. Aura was launched on July 15, 2004 into the A-Train formation, flying eight minutes behind Aqua. TES is an infrared, high-resolution Fourier transform spectrometer. Global surveys are made roughly every other day, and with a spatial coverage of 5.3 km

by 8.5 km in the nadir (and approximately 180km between successive nadir observations), a full global survey requires approximately 16 days or 233 orbits (Beer et al., 2001).

The retrieval algorithm for TES uses the optimal estimation approach as described by Rodgers (2000). The retrieved CO volume mixing ratio ($\hat{\mathbf{x}}$) is expressed as the linear combination of the true profile weighted by the averaging kernel (**A**) and the a priori profile ($\mathbf{x_a}$), along with the spectral measurement error ($\boldsymbol{\mathcal{E}}$).

$$\ln \hat{\mathbf{x}} = \ln \mathbf{x_a} + \mathbf{A}(\ln \mathbf{x} - \ln \mathbf{x_a}) + \boldsymbol{\varepsilon} \qquad \textbf{(Equation 1)}$$

The averaging kernel is a measure of the sensitivity of the retrieval to the true state of the atmosphere, and its trace, also known as the degrees of freedom (DOF), tells how many statistically independent elements of information were available from the measurements to calculate the profile. Full TES CO profiles generally have 1-1.5 pieces of information in the troposphere (Luo et al., 2007; Parrington et al., 2008). Retrieved profiles with low DOFs are dominated at most levels by the a priori profile, which is generated from MOZART CTM output of monthly mean mixing ratios averaged over 10º latitude by 60º longitude bins.

For this work, we are using Level 2, Version 004 Global Survey nadir observations of CO for December 2006 through November 2007. We primarily use daytime observations because of the heightened vertical resolution in the lower troposphere due to increased thermal contrast (Deeter et al., 2007). However, for comparisons with CALIOP during specific transport events, we do include several night observations. We also filter the data using the recommended ranges for Quality Flags for CO (Osterman et al., 2007).

2.2 In situ Observations: IMPROVE network

The Interagency Monitoring of Protected Visual Environments (IMPROVE) was initiated in 1987 with the goal of implementing a network of stations to monitor visibility conditions and to attempt to determine the cause of visibility degradation at each site (Malm et al., 1994). Measurements are taken over a 24 hour period once in three days and are analyzed for the concentration of fine and total particle mass, optical absorption, and the presence of major and trace elements, including sulfate, nitrate, and elemental and organic carbon. There are currently over 100 sites in the United States, located mainly in National Parks and Wilderness Areas.

Previously, Park et al. (2004) used data from 2001 at 141 stations to show that the GEOS-Chem model simulation of sulfate was unbiased (R^2=0.91 annually, slope=0.91). For this work, we use the sites located at Mount Rainier National Park and White Pass in Washington to determine the impact of Asian plumes on surface sites on the west coast of the United States (Figure 2.2). Although they are only separated by 60km (and therefore in the same model grid box), Mount Rainier has a surface elevation of 427 m while White Pass has an elevation of 1830 m. This allows us to make some comparisons between incoming plumes at different altitudes.

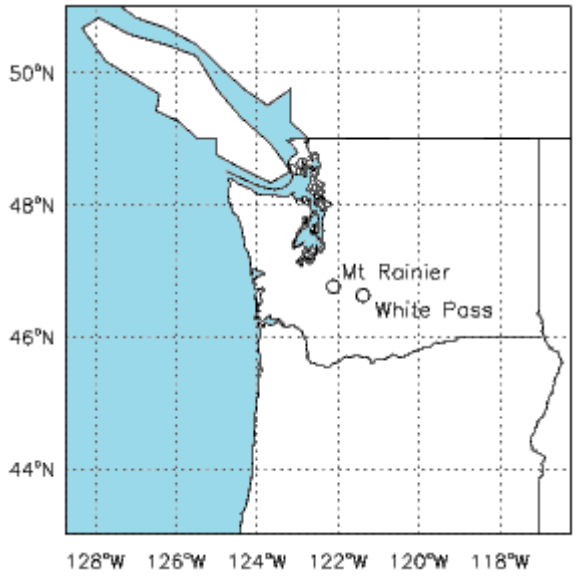

Figure 2.2: Location of White Pass (elevation 1827.33m) and Mount Rainier (elevation 439m) IMPROVE stations.

2.3 GEOS-Chem Simulation

GEOS-Chem is a global three-dimensional, chemical transport model (CTM) driven by assimilated meteorological observations from the NASA Goddard Earth Observing System (GMAO). For this work, we use GEOS-Chem version 8-01-04 (http://geos-chem.org) with the native meteorology at 0.5º latitude by 0.67º longitude horizontal resolution reduced to a 2º latitude by 2.5º longitude and 47 vertical levels for computational expediency.

This simulation includes tropospheric ozone-nitrogen oxides-hydrocarbon chemistry coupled with aerosol chemistry through inorganic aerosol formation (sulfate, nitrate, ammonium), heterogenous reactions (Evans and Jacob, 2005), and effects on photolysis rates (Martin et al., 2003). Aerosol simulations also include carbonaceous aerosols (Park et al., 2003), dust (Fairlie et al., 2007), sea salt (Alexander et al., 2005),

and secondary organic aerosols (SOA) (Chung and Seinfeld, 2002; Liao et al., 2007). Aerosols and gases are removed by both wet and dry deposition in the model. The wet deposition scheme includes scavenging in convective updrafts, rainout and washout (Liu et al., 2001), while dry deposition of gases and aerosols is dependent on surface characteristics and meteorological conditions (Wesley, 1989). Aerosol optical depths (AOD) at 550nm are calculated from the mass concentration and the extinction coefficient for each aerosol type following Martin et al. (2003), with updated aerosol size distributions as described in Drury et al. (2010). We do not attempt to account for differences between the model and satellite assumed aerosol optical properties here.

Anthropogenic emissions are based on the GEIA inventory (Benkovitz et al., 1996), with emissions of nitrogen oxide (NOx), CO, and sulfur oxide (SOx) based on the EDGAR emissions inventory (Olivier, 2001a; 2001b). These global estimates are overwritten by several regional inventories, such as CAC for over Canada (http://www.ec.gc.ca/pdb/cac/cac_home_e.cfm), BRAVO over Mexico (Kuhns et al., 2003), EMEP over Europe and for ship exhaust (Vestreng et al., 2007), EPA NEI99 over the USA which is also used for biofuel (Hudman et al., 2007; 2008) and the Zhang et al. (2009) inventory for southeast Asia. Biogenic VOC emissions are calculated interactively following MEGAN (Guenther et al., 2006). Global anthropogenic emissions of black and organic carbon follow Bond et al. (2004) with the exception of North America, where emissions of these species follow Cooke et al. (1999). Biomass burning and biofuel emissions are specified according to the GFED2 (van der Werf et al., 2006) and Yevich and Logan (2003) monthly inventories.

A series of simulations were performed for this work. A full, online chemistry simulation was run as a baseline simulation for comparison. Separate sensitivity runs were then conducted to determine the impact of emissions from North America, Asia, and Europe on the Northern Hemisphere by shutting off all emissions in a given region (Figure 2.3). This allows us to distinguish locally produced enhancements from background concentrations.

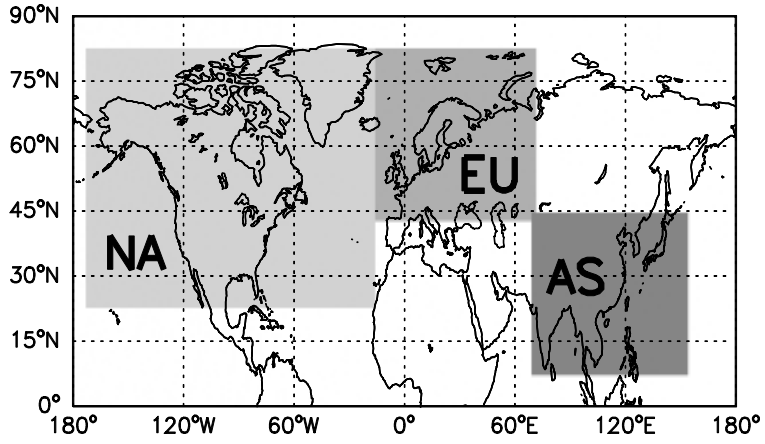

Figure 2.3: Emission Regions in the Northern Hemisphere: North America (NA), Europe (EU), and Asia (AS).

All simulations are conducted for December 2006-November 2007 with initialization on December 1 after an eight-month spin-up simulation. Daily diagnostics are output to coincide with A-Train overpass time, averaged from 1-2 local time for nighttime and 13-14 local time for daytime overpasses. We first re-grid all the satellite data to the standard GEOS-Chem 2º by 2.5º grid as depicted in Figure 2.4 where we take a satellite (CALIOP) observation track (Figure 2.4a), separate all the observations into the corresponding GEOS-Chem grid box (Figure 2.4b), and determine an average AOD for each grid box for the date and observation period (Figure 2.4c). After re-gridding the

satellite data, we then sample the GEOS-Chem output along the satellite observation track by only using grid boxes with valid observations. Also to note from Figure 2.4b, AOD from CALIOP used here for comparisons with GEOS-Chem are actually an average of approximately 20 observations. For TES, we also linearly interpolate the model profile to the 67 valid TES pressure levels before applying the retrieval operator as in Equation 1.

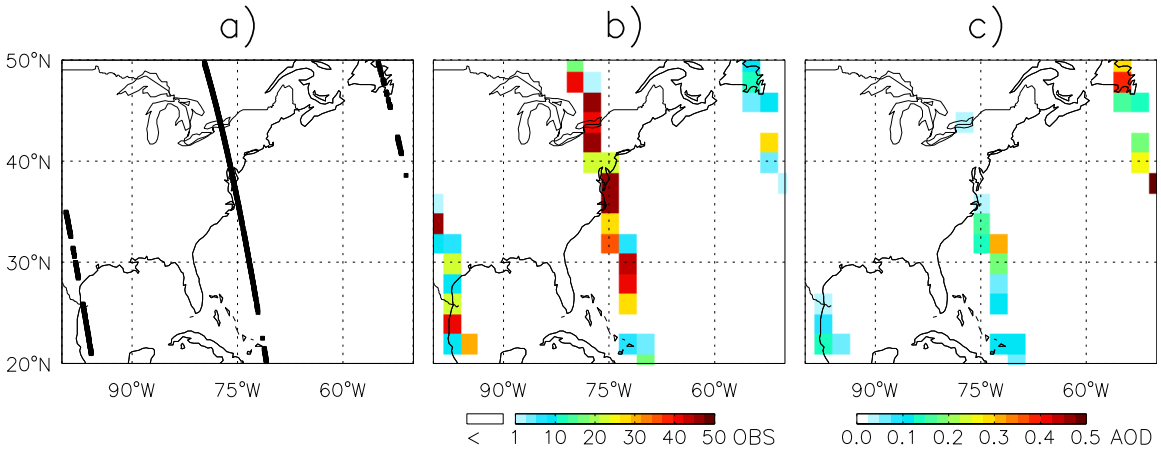

Figure 2.4: Example of re-gridding CALIOP observations to the GEOS-Chem, where a) shows the original satellite track for the night observation, b) shows the number of CALIOP observations in each GEOS-Chem grid box and c) shows the final averaged AOD to which GEOS-Chem will be compared.

We made initial comparisons between CALIOP and GEOS-Chem distributions of AOD from corresponding grid boxes as shown in Figure 2.5. The majority of observations from CALIOP are for AOD values of 0, whereas GEOS-Chem never simulates an AOD of 0, since there are always some aerosols in an atmospheric column. The great majority of AOD values of 0 can lead to a low bias in AOD estimates in regions with already low loadings. However, while CALIOP has more low values, it also has a wider range of values compared to GEOS-Chem (because GEOS-Chem values are

average values for a gridbox), with several large outliers, showing no systematic high or low bias for all the data.

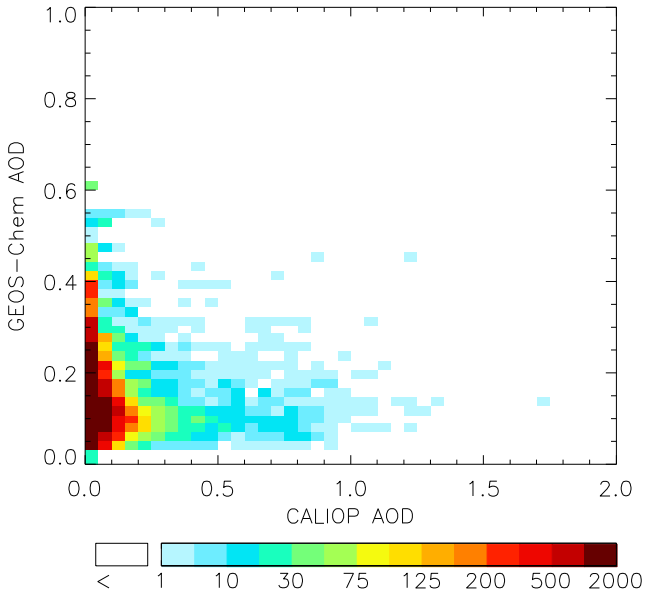

Figure 2.5: Plot of the distribution of CALIOP AOD and corresponding GEOS-Chem grid box AOD. Color bar is saturated at 2000 observations.

However, it is also important to note that any comparison made with satellite data (CALIOP, MODIS or TES) will only use data for when the satellite had a valid retrieval. Therefore, our comparisons are limited to what a satellite observes and may not be completely representative of the full atmospheric state. This issue is discussed further in subsequent chapters.

3 Potential Issues when comparing GEOS-Chem and satellite observations

Although we attempt to match model output with observations for comparison, because we are attempting to look at long range transport events that happen on timescales of several days, the limited spatial coverage of satellites with small footprints such as TES and CALIOP can pose several challenges. While the model may indicate a distinct plume being transported, the satellite may not observe over the region for that day as shown in Figure 3.1a, where for March 24th, 2007, GEOS-Chem predicts high AOD values over the North Atlantic due to a plume being transported off the east coast of North America, yet, the CALIOP track for the day misses all but the edges of the plume. On seasonal scales, sampling of the model along the satellite track does not bias the average extinction profile as seen in Figure 3.1b, which shows that using all data for Spring 2007 over the boxed region in Figure 3.1a, produces an almost identical profile to sampling only when there was a valid satellite observation over the region. However, when we examine the time series of the average AOD for the same region (Figure 3.1c), several transport events, such as the plume on March 24th, are missed because they are sampled out. This implies that comparisons of model simulations with satellite observations with no cross-track scanning (as in CALIOP and TES) are particularly susceptible to model transport errors, meaning that misplacement of a plume potentially due to advection that is too strong or too weak can dramatically skew any similarities when examining limited observational areas. These issues will be shown in greater detail in Chapter 4.

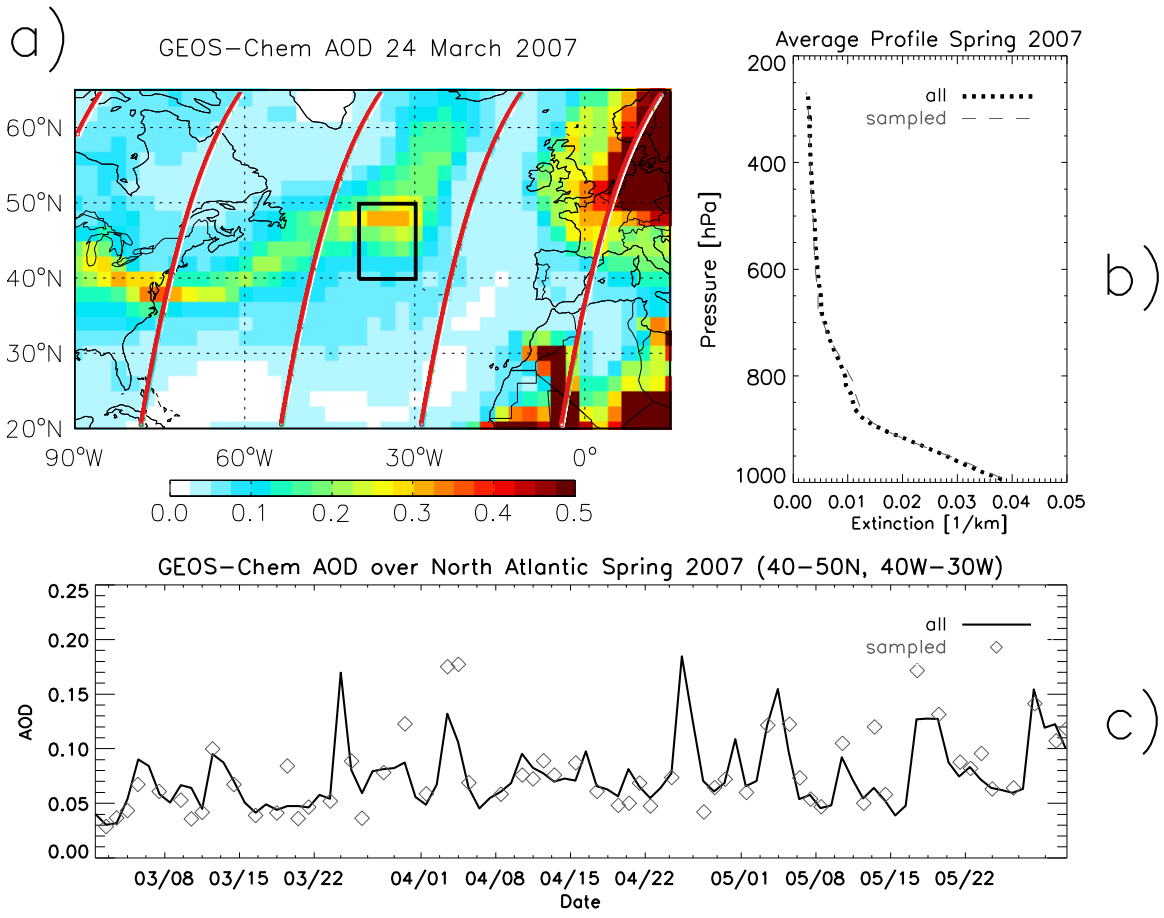

Figure 3.1: Plots depicting sampling issues: a) AOD from GEOS-Chem with the track for CALIOP (red) and the box for averaging; b) average spring extinction profile for GEOS-Chem (dotted) and when sampled to the A-Train path (dashed); c) time series of the total column AOD for spring 2007 from GEOS-Chem (solid) and when sampled (diamonds).

In addition to these sampling issues, previous studies have noted specific biases when comparing GEOS-Chem with these satellites. While MODIS AOD is found to have generally good spatial agreement with GEOS-Chem, it was found to be biased high over the Pacific, particularly at low loading (Heald et al., 2006), and over land, notably in the western US (Li et al., 2005; van Donkelaar et al., 2010). This bias has mainly been attributed to application of the land algorithm over varying surface terrains. Generosa et al. (2008) used CALIOP backscatter profiles and AOD from MODIS to examine dust

transport across the Atlantic and compare with GEOS-Chem. They found that model-derived backscatter profiles and CALIOP agreed qualitatively on plume layer heights, but that the model over predicted AOD near the source and under predicted AOD downwind, suggesting either too little transport or too much removal. van Donkelaar et al. (2010) also compared GEOS-Chem and CALIOP relative profiles to show that, although AOD values do not agree, there are similarities in the distribution of AOD. Finally, for CO, Kopacz et al. (2010) found that while GEOS-Chem has higher correlations and fewer differences with TES than MOPITT or AIRS, simulated CO column totals are still biased low.

4 Examining an event of long range transport: May 14th, 2007

We choose a transport event from North America to Europe which, according to GEOS-Chem output, occurred over the time period of March 14th to March 16th, 2007. The spatial distribution is analyzed through the column AOD and column concentrations of carbon monoxide due to North America emissions (from the sensitivity runs). Figure 4.1 shows export from the Northeastern US with high column AOD on March 14th. Due to an anticyclone in the North Atlantic and a cyclone in Northern Canada, the polluted air mass was quickly transported north eastward on the 15th and then southward on to the British Isles on the 16th. The spatial pattern of simulated column concentrations for CO (not shown) are quite similar; however, due to the longer lifetime of CO compared to aerosols, and thus higher background concentrations, the plume is not as well defined.

For making spatial comparisons, MODIS is generally better than CALIOP because it has a much larger footprint. Unfortunately, as MODIS cannot see through clouds, anytime clouds and aerosols are mixed, as often occurs in the case of lofting, no values are available. For this transport event, MODIS detected some high AOD values at the source and along the edge of the area where GEOS-Chem had simulated the plume (Figure 4.2). While it is difficult to determine the agreement of plume location and intensity with these scattered values, they suggest that the aerosol plume may be coincident with clouds as often occurs with export in frontal systems (Kulmala et al., 2006).

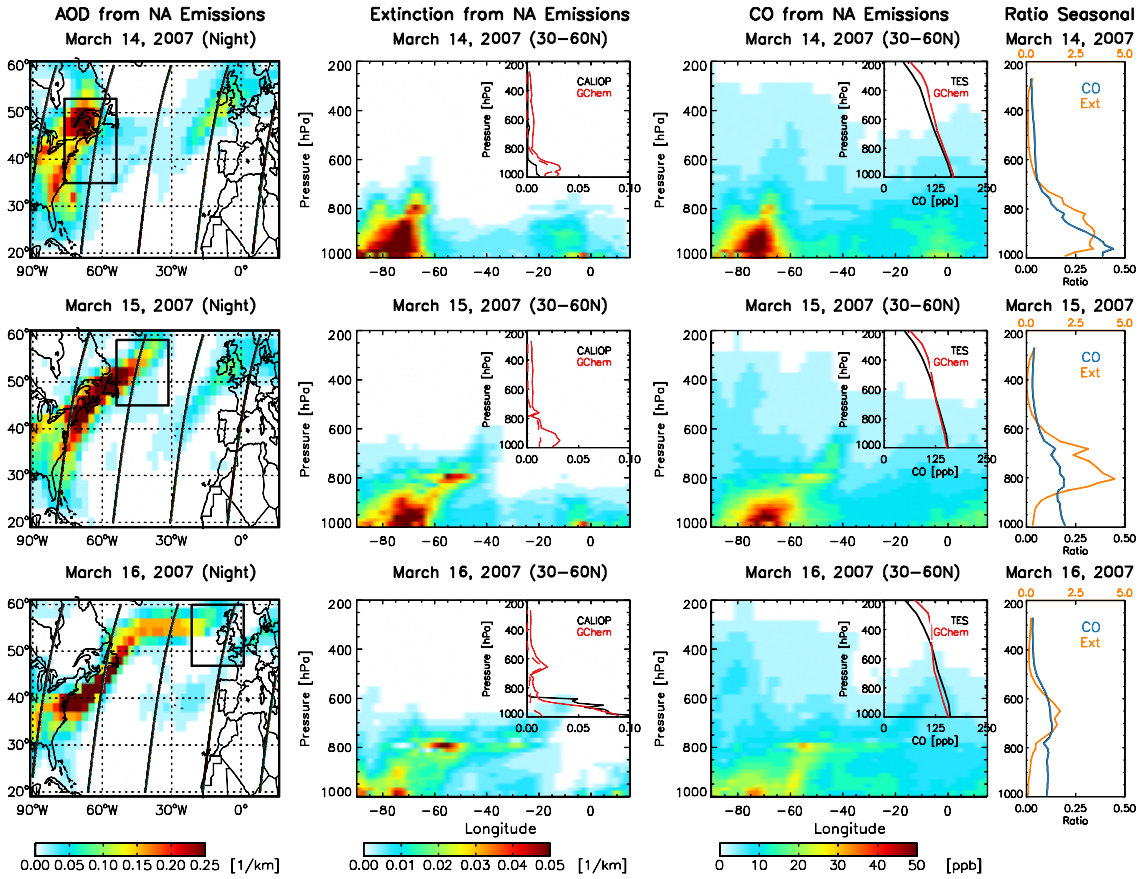

Figure 4.1: Column 1 is the simulated AOD from GEOS-Chem due to North American emissions. Black line is the overpass path for CALIOP and TES. Column 2 (3) is the simulated vertical distribution of extinction (CO) due to emissions. Inset plot shows the average profile for the boxed region in Column 1 observed from CALIOP (TES) in black, full GEOS-Chem in solid red, and dashed red is for tagged North American emissions. Colum 3 shows the ratio of that profile to the seasonal mean. Rows are organized by date.

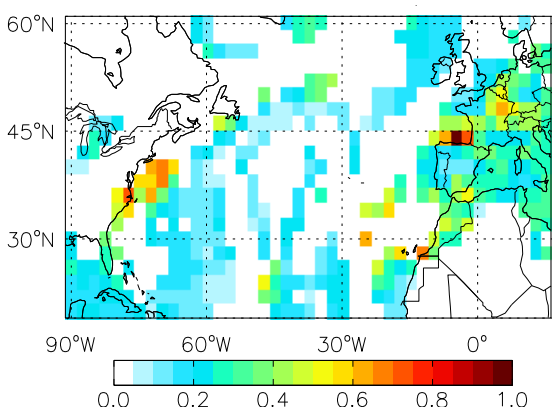

Figure 4.2: AOD from MODIS March 15, 2007.

To better understand how this air mass was transported and its final impact on its destination region, we then examine the vertical distribution of CO and aerosols during transport (2nd and 3rd columns of Figure 4.1). Both CO and aerosols are lofted above 800hPa during export from North America. We see this lofted plume moves across the mid-Atlantic on the 15th and finally reaches the British Isles on the 16th. This elevated plume appears to be the only major aerosol plume in the GEOS-Chem simulation; however, the CO export in the model consists of both an upper level plume and boundary layer export. This difference is consistent with the previous simulated difference in springtime transpacific aerosol and CO transport (Heald et al., 2006) and is also depicted by the ratio of the single day emission profile to the seasonal average profile (Figure 4.1, column 4), where the aerosol enhancement away from source is in a distinct lofted layer, whereas the CO is enhanced throughout the column.

The insets of Figure 4.1 show the comparison with the average CALIOP aerosol extinction and average TES CO profiles over the region. On the fourteenth, CALIPSO passed over the northeast coast, where GEOS-Chem predicts high AOD values. However, it only catches the edge of the plume and has significantly lower extinction values. The

TES CO profile and the transformed GEOS-Chem simulated CO profiles appear to be in agreement; however, both of these profiles are relatively uniform given the inability of IR sounders to retrieve significantly more than 1-2 pieces of information in the vertical.

Although CALIPSO did pass over the region where GEOS-Chem showed a plume being transported across the North Atlantic on the 15th, there were no valid retrievals (using the aforementioned filtering). As with MODIS, the issue is most likely due to a coincidence with clouds. As noted by Liu et al. (2009) and Yu et al. (2010), thick aerosol layers near source regions are often misclassified by the CAD algorithm. As shown in Figure 4.3, CALIOP observed significant cloud layers on the 14th and 16th; and while it only observed an optically thin layer on the 15th, there were also significantly fewer valid observations.

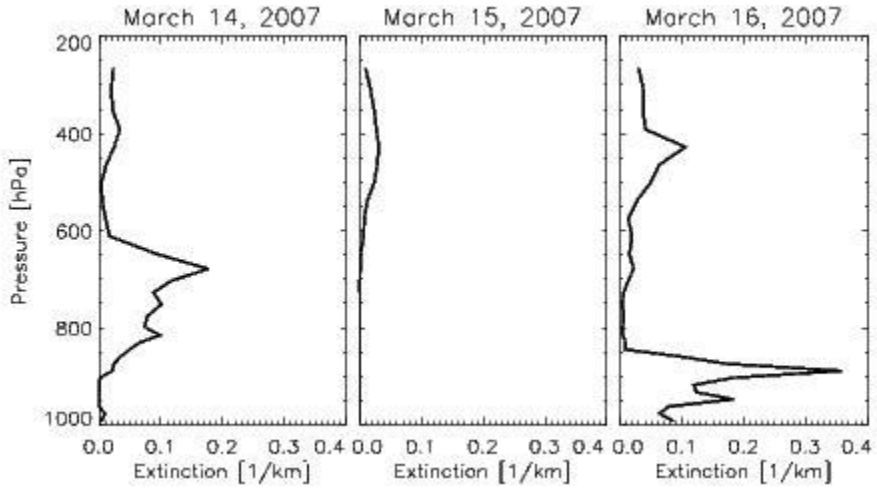

Figure 4.3: CALIOP Cloud extinction profiles for March 14-16th, 2007.

By the sixteenth, there is less lofting of aerosols from the surface at the emission source as a high has moved northwest of the Atlantic seaboard. Vertically, the plume is not as well defined, and seems to have fragmented. Farther downwind, there is a localized maximum over 30W to 15W at about 800hPa, but without the plume

descending at the receptor region, it has no surface impact. This is also evident in the extinction profile where there is a lofted layer of high extinction that is due to the influence of North American emissions (dashed line), but only a small contribution of the total surface layer extinction due to transport.

CALIOP does make observations over the British Isles on the 16th and measures high extinction values up to around 850hPa, in very good agreement with the simulated profile from GEOS-Chem (Figure 4.1, Row 3). The model seems suggests that most of this lower enhancement is due to local emissions rather than transported North American emissions and CALIOP does not show an upper level enhancement like GEOS-Chem (~600hPa). Because there are no valid profiles for the transport region on the 15th, it is difficult to determine if CALIOP is invalidating the transport or perhaps suggesting the plume descended further.

These satellite instruments can provide us with some information on vertical distributions during export and transport events. However, the small footprints and limited number of valid observations, make it difficult to determine broad characteristics about transport in each region from daily observations, which is why we choose to analyze LRT on seasonal timescales in subsequent chapters.

5 Seasonal Features of Long Range Transport in the Northern Hemisphere

5.1 Spatial Distributions of Pollutants

5.1a Column Concentrations of Aerosols and CO

Prior to investigating the vertical distribution of pollution transport, we compare here the spatial patterns of simulated AOD and CO column with satellite observations to confirm the reliability of the model representation of source regions and transport.

Atmospheric aerosols are the result of primary emissions and chemical transformations of precursors from both natural sources, such as volcanoes and desert dust, and anthropogenic sources, such as vehicle emissions, agricultural burning, and power plants. Figure 5.1 shows the spatial distributions of AOD as observed by MODIS and CALIOP and as predicted by GEOS-Chem. In general, the observations and model give a consistent picture of the major source regions such as East China, the Eastern US and the dust region in western Africa. However, in export regions (off western Africa, off Asia, and off the Eastern US), GEOS-Chem AOD is often lower in magnitude than both MODIS and CALIOP.

While there are noted issues with the simulated dust transport off western Africa in GEOS-Chem (Generosa et al., 2008), here we choose to focus on export out of industrial regions in the mid-latitudes where the transport of aerosols has the greatest potential to impact downwind air quality. We do note that dust from Africa does

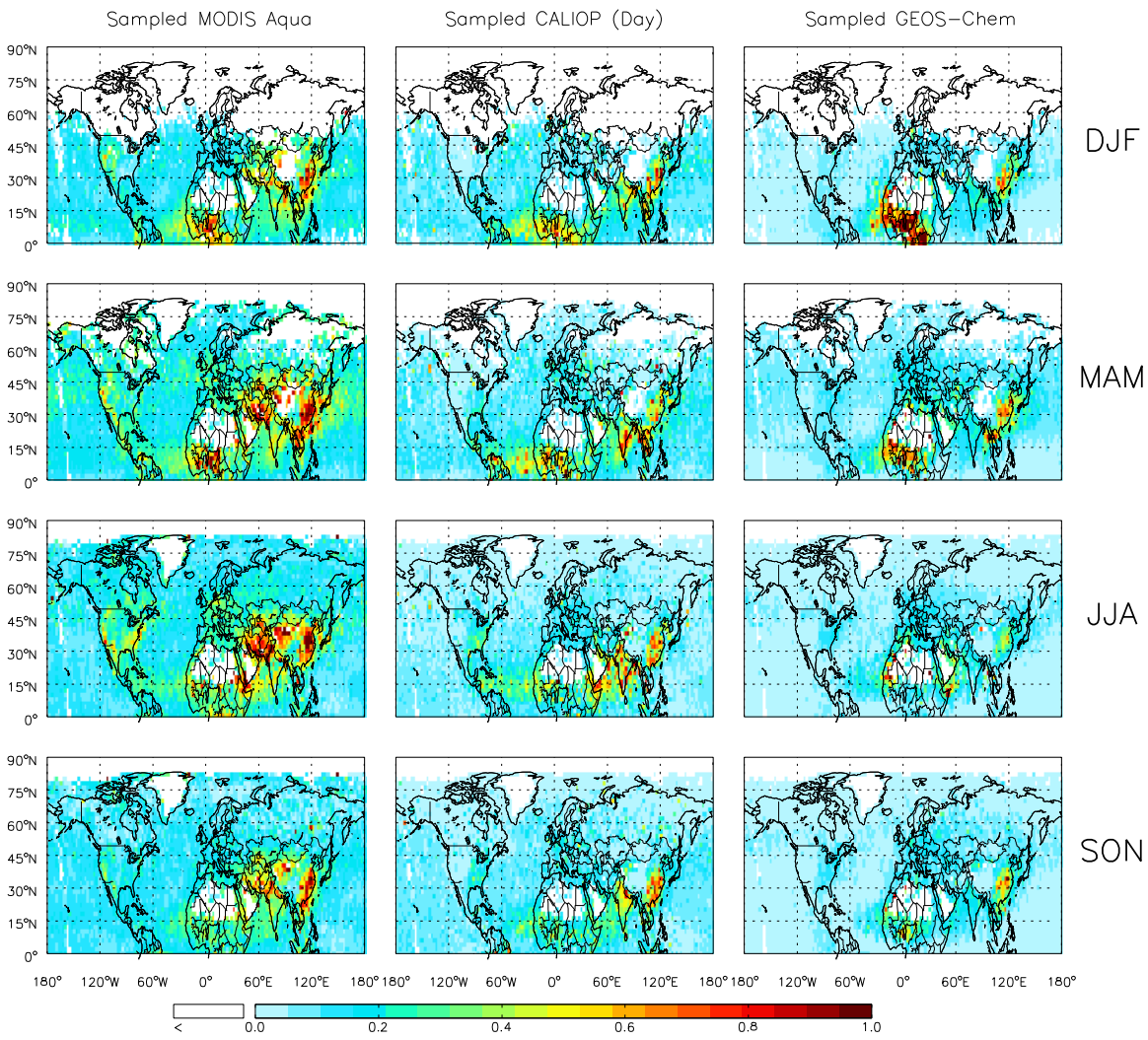

Figure 5.1: Seasonal averages (organized by row) of aerosol optical depth as observed by MODIS Aqua (Column 1), CALIOP (daytime observations, Column 2), and as simulated by GEOS-Chem (Column 3); all are sampled for valid MODIS and CALIOP observations. The color bar is saturated at 1.0.

contribute to AOD over Europe (and sometimes over the US) and could lead to slightly higher simulated AOD values; however, this appears to make a relatively small contribution in GEOS-Chem.

MODIS is generally higher over the oceans than both CALIOP and GEOS-Chem, in agreement with previous studies that suggested that MODIS might be biased high at

low loadings (Heald et al., 2006; Remer et al., 2005; Levy et al., 2005). Kittaka et al. (2010) also found that, outside tropical regions, MODIS AOD is higher than CALIOP over oceans. Over land, at low latitudes, CALIOP AOD is higher; while at mid-latitudes, MODIS is higher. They noted several other regional and seasonal biases of both signs, but overall, found that the global mean AOD from CALIOP was biased low in comparison to MODIS. GEOS-Chem is also much cleaner than CALIOP over the oceans, and the underestimate of AOD from both of these instruments could suggest there is too much removal in the model near sources. This, however, is difficult to determine from column totals and will be investigated further through vertical distributions.

The model also captures the seasonal evolution of export from the major Northern Hemisphere source regions. The greatest outflow from Asia is in the spring; although, compared to the other regions, there is substantial export in all seasons. Outflow from the eastern US also occurs in all seasons, though based on the observations here, the pathways are different. In fall and winter, aerosols are transported at higher latitudes than in spring and summer. European emissions tend to remain more localized and export is therefore difficult to distinguish from local emissions in most seasons. The exception is for spring, where MODIS, CALIOP and GEOS-Chem all show higher AOD values over the high latitudes (~60-75N), which are indicative of transport to the Arctic. This is a challenge to confirm observationally given the inability of satellites to retrieve over snow-covered surfaces.

We contrast aerosol transport with that of CO, a gas-phase pollutant and precursor to ozone formation which is relatively insoluble and has a several month lifetime against oxidation by OH (Levy, 1974). Because of its moderate lifetime and less complex

chemistry, CO has been frequently used as a tracer for long range transport (Reidmiller et al., 2009). Figure 5.2 compares column totals of CO concentrations from TES and GEOS-Chem (with the TES retrieval operator applied as described in Chapter 2), and shows that this long lifetime enhances background concentrations of CO hemispherically.

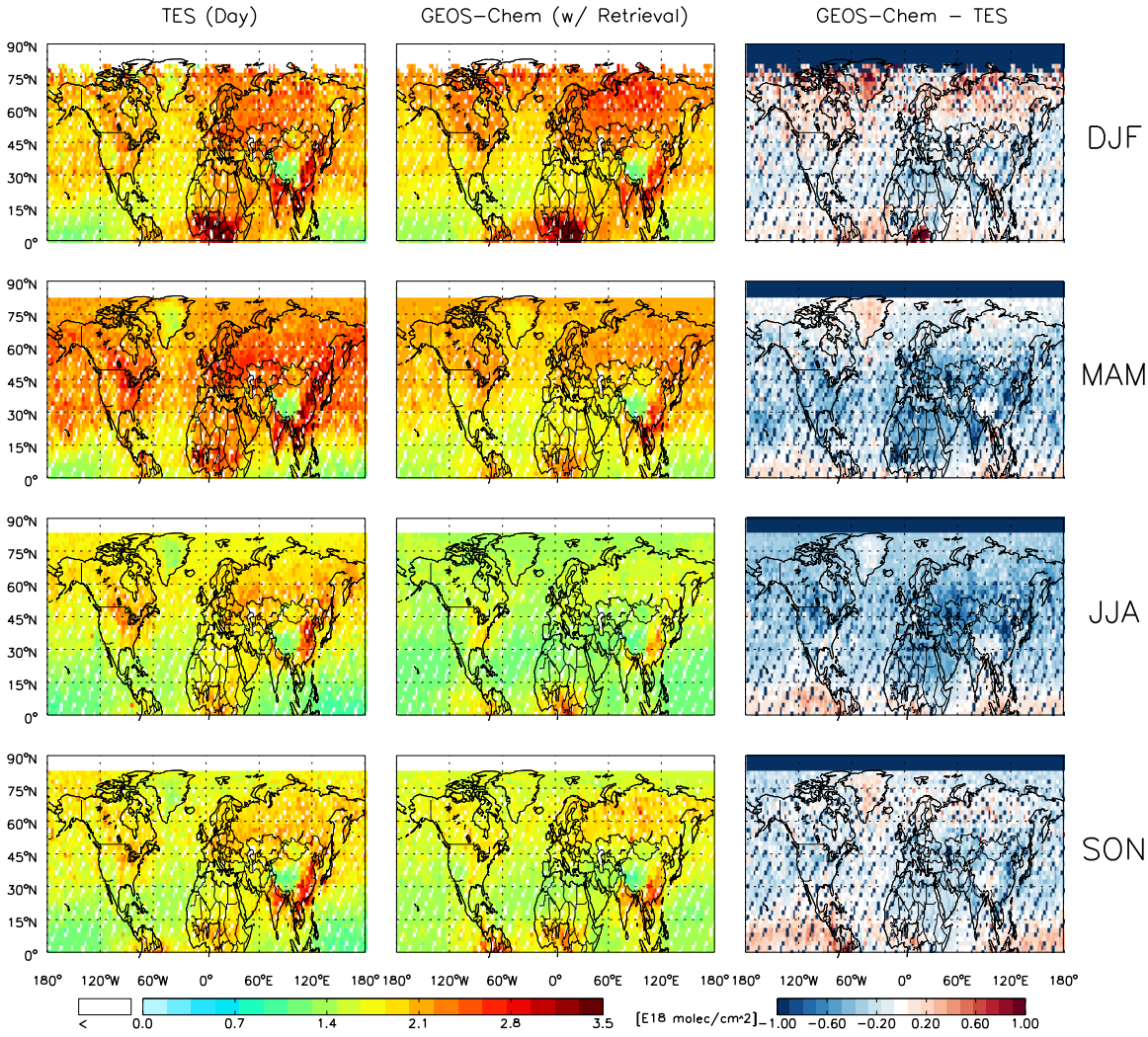

Figure 5.2: Seasonal averages of CO column concentrations from TES (Column 1), GEOS-Chem with the TES operator retrieval applied (Column 2), and the difference (GEOS-Chem minus TES, Column 3). The GEOS-Chem simulation is sampled for TES overpass times and locations. Color bars are saturated at 3.5×10^{18} molecules/cm² and $\pm 1 \times 10^{18}$ molecules/cm² respectively.

As previously mentioned, GEOS-Chem is generally lower than TES, especially over source regions and the differences are greatest in spring and summer (Kopacz et al., 2010). However, both model and observations can be used to identify the major source regions and highlight the seasonality in the atmospheric oxidant loading, which in several regions, appears to overwhelm the seasonality in emissions for determining column totals, such as for comparison between winter and spring for the eastern US. In the eastern US and Europe, emissions are slightly higher in the summer with increased summer travel, while in other parts of the world, changes in emissions are mainly due to biomass burning. Yet, transport seems to be uniformly more apparent in winter and spring when stronger winds advect pollution more efficiently.

5.1b Emissions of Aerosols and CO

In order to distinguish export from and transport to each region from background concentrations, we examine a series of sensitivity simulations from GEOS-Chem. Figure 5.3 shows the seasonal averages of AOD due only to emissions from North America, Europe, and Asia, respectively. We clearly see that Asian emissions have the largest hemispheric influence, although transport occurs in all seasons from all emission regions. Most transport in the mid-latitudes follows the mean zonal wind, and as such, Asian emissions are generally transported eastward towards the west coast of North America and in most seasons, aerosols are transported across North America to Europe. However, there is also transport northward to the Arctic and the Middle East from Europe. Figure 5.3 is consistent with previous studies which suggest that only a small fraction of emitted aerosol are transported intercontinentally, perhaps limiting impacts on downwind air quality (Park et al., 2004; Liu et al., 2009a).

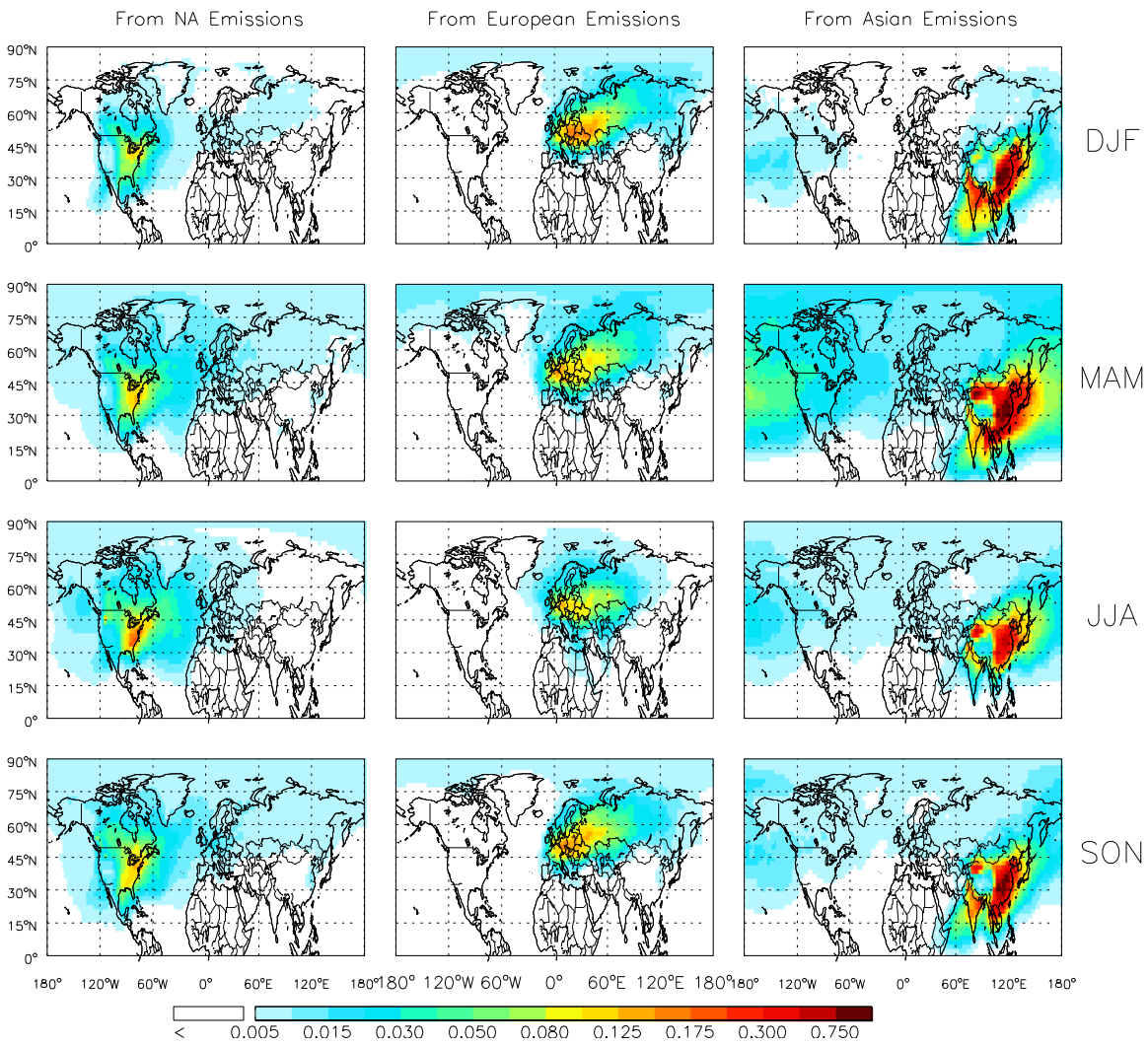

Figure 5.3: Seasonal maps of column AOD resulting from each emission region as simulated by GEOS-Chem. The color bar is saturated at 0.75. Note the non-uniform scaling of the color bar.

North American aerosol pollutants primarily move northeast towards Europe with a small percentage transported as far as eastern Russia. Unlike Europe and Asia, where transport is most pronounced in spring, for North America, summer is also a season of increased transport, partly due to the fact that it also is a season of high emissions.

European emissions have three distinct transport pathways as noted by Duncan and Bey (2004) and as evident here. The most dominant export is towards the northeast over Russia, which can also lead to transport to the Arctic, where it is notably the cause

of Arctic haze (Quinn et al., 2007; Stohl et al., 2002). In the spring, this pollution also makes it to the northernmost part of North America. There is also some transport westward over the North Atlantic (2^{nd} pathway) and across the Mediterranean Sea towards North Africa (3^{rd} pathway), but we will focus on the first pathway as it is the most dominant and efficient export from Europe in the mid-latitudes. In addition, the second and third pathways track over regions with significant local emissions and are therefore harder to distinguish from observations. There is a seasonal cycle to this pathway as evident in Figure 5.3, where export in fall, winter, and spring primarily follows this trajectory towards the northeast and then over the Arctic. In summer transport is more zonal, and exerts little influence over the polar region. Many previous studies have noted that while pollution export from Europe has the greatest potential to impact downwind sites due to its close proximity to other continents, the mechanisms for export are less efficient (Stohl et al., 2002). However, this is difficult to ascertain from spatial distributions and will be more evident from vertical distributions.

As for species emitted in GEOS-Chem, inorganic aerosol (primarily sulfate aerosol [Park et al., 2004]) is the dominant contributor for AOD from North America and European emissions (Figure 5.4), accounting for more than 90% in most regions. For Asia, although sulfate still dominates AOD, dust is also a large contributor, especially in the spring in the Taklamakan and Gobi desert regions (Figure 5.5). Edwards et al. (2004) noted that because sulfate is the dominant contributor to fine mode AOD and is primarily produced through oxidation of sulfur dioxide (SO_2) and hydrogen peroxide (H_2O_2), seasonality of observations of AOD also depends on the oxidizing capacity of the atmosphere, and generally lags peak CO by several months in many regions.

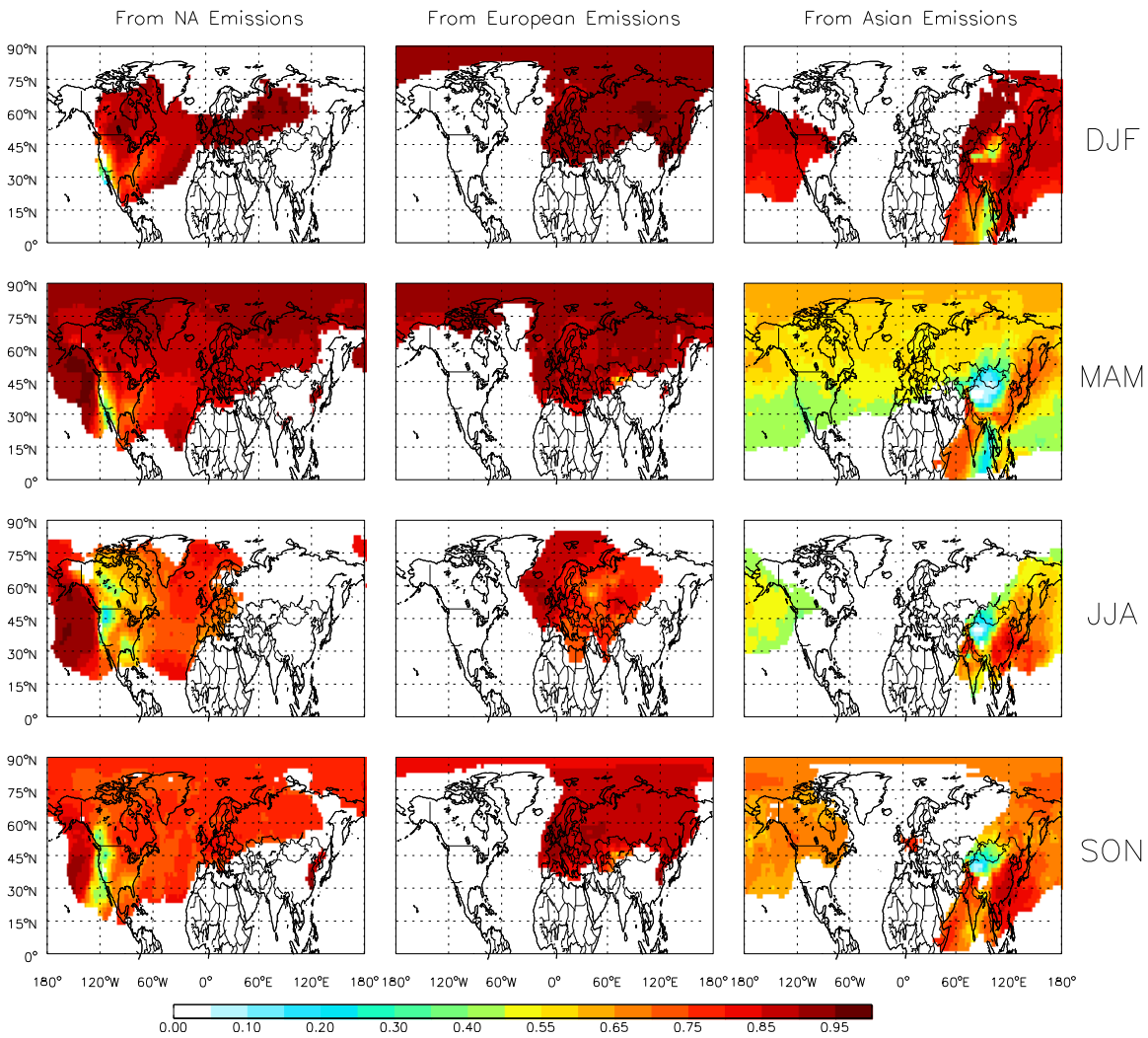

Figure 5.4: Maps of the fraction of seasonal AOD that is due to inorganic aerosol (primarily sulfate). The color bar is saturated at 0.95.

The spatial distributions of CO tagged by emission regions in Figure 5.6 show many similar source regions as particulates, once again highlighting the eastern US, western Europe and China. As with aerosols, Asia is the most copious source of CO in all seasons, although GEOS-Chem predicts that in every season, there will be a small contribution to the background concentration of CO in almost every region of the Northern Hemisphere due to emissions from all three source regions. However, sulfate has an atmospheric lifetime of ~2-5 days (Rasch et al., 2000) compared to weeks or

months for CO. Therefore, transported CO consists of both fresh and aged air masses, making it challenging to distinguish individual transport events.

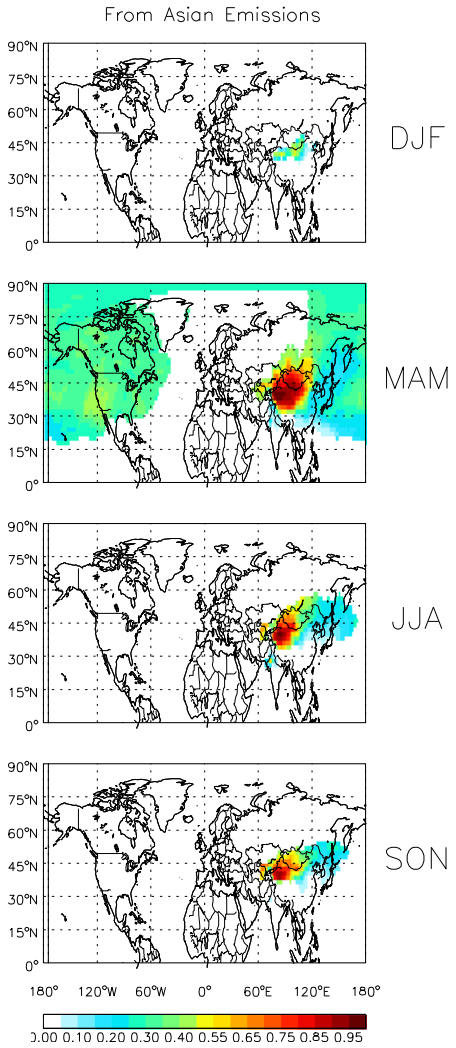

Figure 5.5: Maps of the fraction of seasonal AOD that is due to dust emission from Asia. The color bar is saturated at 0.95.

Due in large part to these lifetime differences along with seasonality in emissions, the seasonal downwind impact of transported aerosols and CO differs considerably. For example, spring is the season where Asian emissions of both CO and aerosols have the greatest impact on the western coast of North America. For North America, CO has the

greatest impact on Europe in fall, when emissions are still high and CO has a longer lifetime, compared to spring and summer for aerosols.

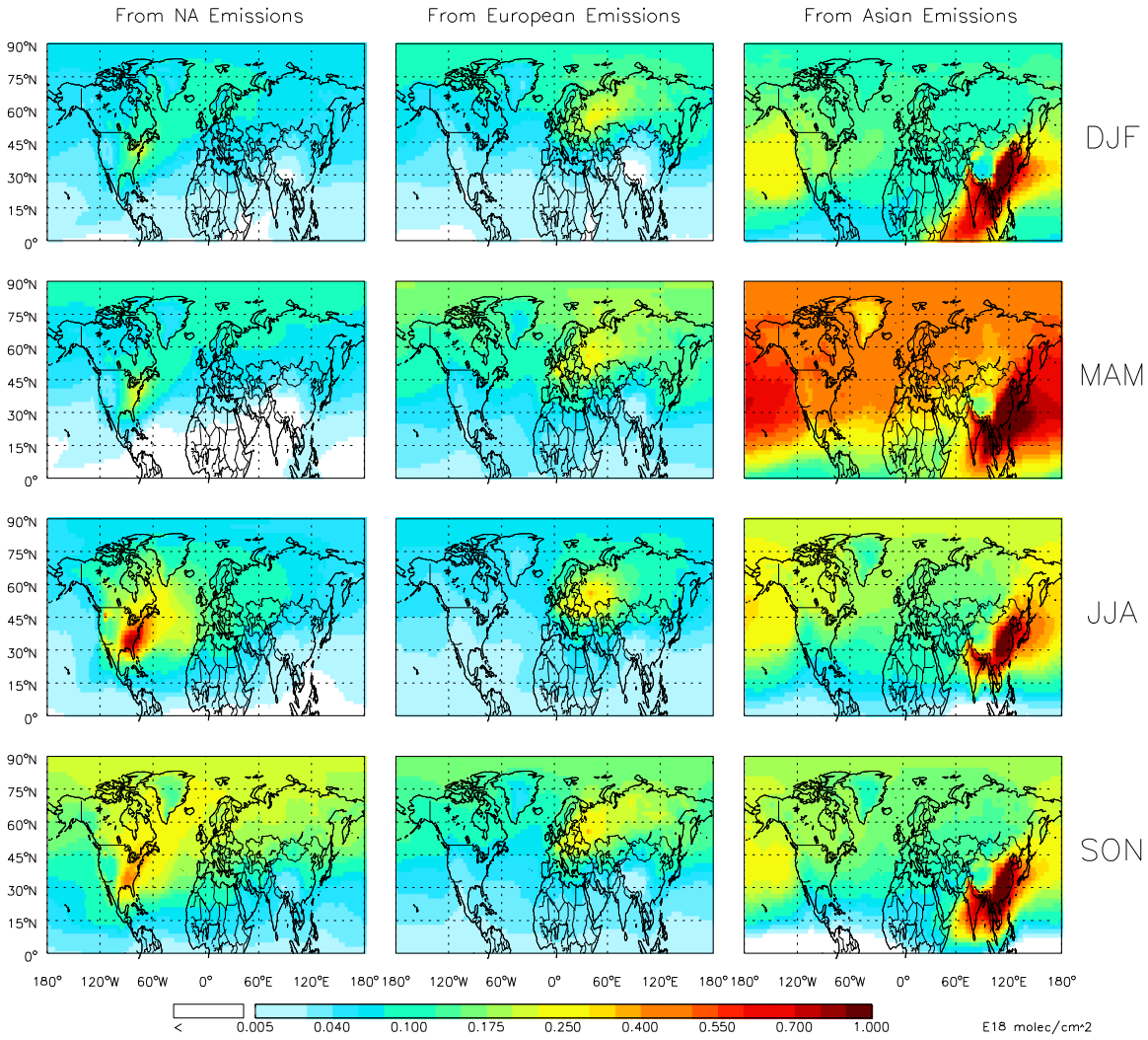

Figure 5.6: Seasonal maps of column concentrations of CO from each emission region simulated by GEOS-Chem. The color bar is saturated at 0.95 x 10^{18} molecules/cm^2.

5.2 Vertical Distributions of Pollutants

5.2a Observational Comparisons

While seasonality in emissions and pollutant lifetimes can account for many of the differences between the downwind impacts of CO and aerosols, there are also

different export mechanisms that are not evident from the total column spatial distributions. We therefore investigate the vertical distribution of LRT here.

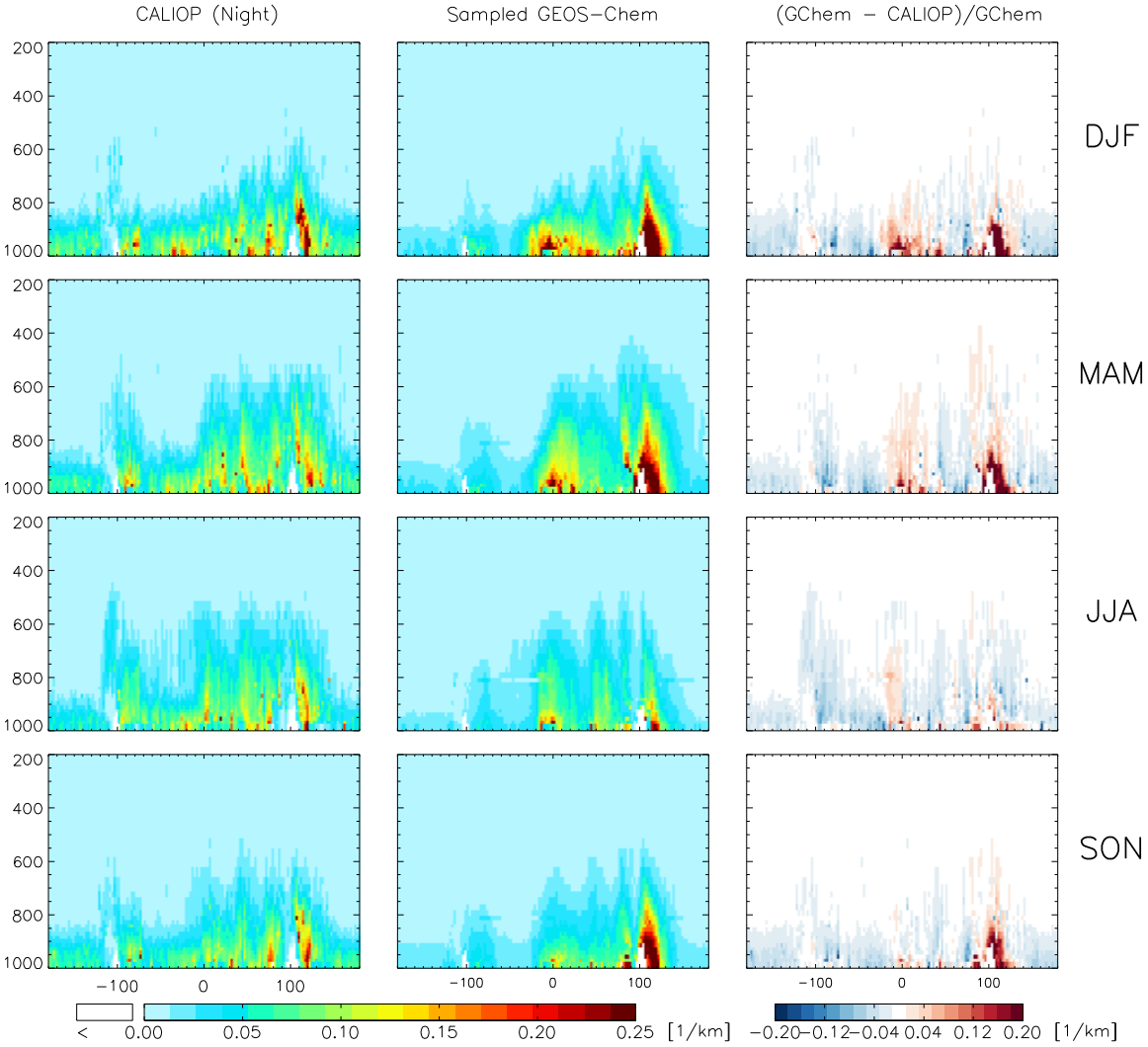

Figure 5.7: Seasonal averages of aerosol extinction averaged from 20-50ºN as observed by CALIOP (night observations only, Column 1) and simulated by GEOS-Chem (Column 2). Column 3 is the difference (GEOS-Chem – CALIOP). GEOS-Chem is sampled to match CALIOP overpass time and location. The color bars are saturated at respective maximum values.

Figure 5.7 shows the seasonal averages of the vertical distribution of aerosol extinction as measured by CALIOP and simulated by GEOS-Chem and the differences. As shown previously, CALIOP and GEOS-Chem tend to agree on source regions.

However, GEOS-Chem seems to be biased high in source regions, as off Asia (at ~90º-120ºE) and over Europe (~0º), but is low in transport regions between sources. GEOS-Chem also has higher lofting directly above sources in Europe and Asia, but less lofting over North America compared to CALIOP.

GEOS-Chem simulates the highest lofting over Asia, although CALIOP does not necessarily support this for all seasons, especially in summer when there is also higher lofting over Europe due to convection (Stohl et al., 2002). These comparisons suggest that CALIOP observations support more efficient export of pollution via boundary layer outflow and advection with the mean wind. Alternatively, GEOS-Chem could be missing some more important background sources in marine regions. One possibility for such a background aerosol would be marine organic aerosol, which is not included in the standard GEOS-Chem simulation. However, these aerosols make up a negligible contribution to AOD and are unlikely to explain the CALIOP observations (Kateryna Lapina, CSU, personal communication).

We also compared vertical distributions of CO as measured by TES and as simulated by GEOS-Chem (with the TES retrieval operator) in Figure 5.8. As discussed previously, GEOS-Chem has an overall low bias compared to TES. This is especially evident over Europe, as seen by Kopacz et al. (2010) who found that European emissions were underestimated in GEOS-Chem. Additionally, GEOS-Chem seems to simulate less CO lofting off China. While again there is agreement in placement of sources, the widespread high bias of TES and coarse vertical resolution of the IR retrieval make it difficult to determine if GEOS-Chem and TES are in general agreement on the vertical distribution of CO. We attempt to investigate this further in the following section.

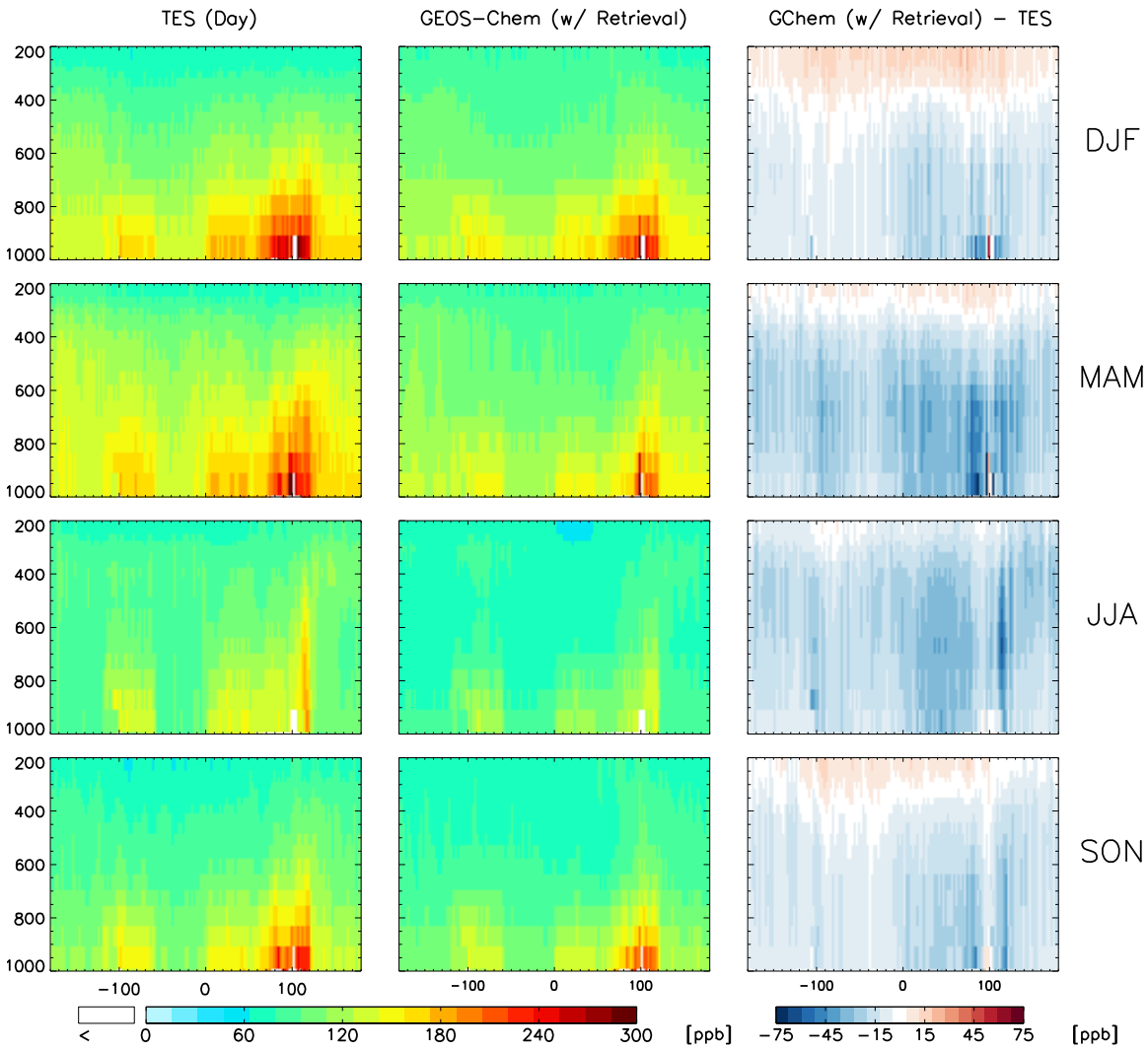

Figure 5.8: Seasonal averages of the vertical distribution of CO from TES (Column 1) and GEOS-Chem with the TES retrieval operator (Column 2). Differences are shown in Column 3. GEOS-Chem is sampled to match TES overpass time and location. The color bars are saturated at respective maximum values.

5.2b Vertical Distribution of Pollutants from Emission Regions

In order to distinguish the source of pollutants, we begin by examining the vertical distributions simulated in the sensitivity runs. This gives us a better sense of the

height of lofting and depth of transported layers out of each region and further insight into where the discrepancies between the model and observations may lie.

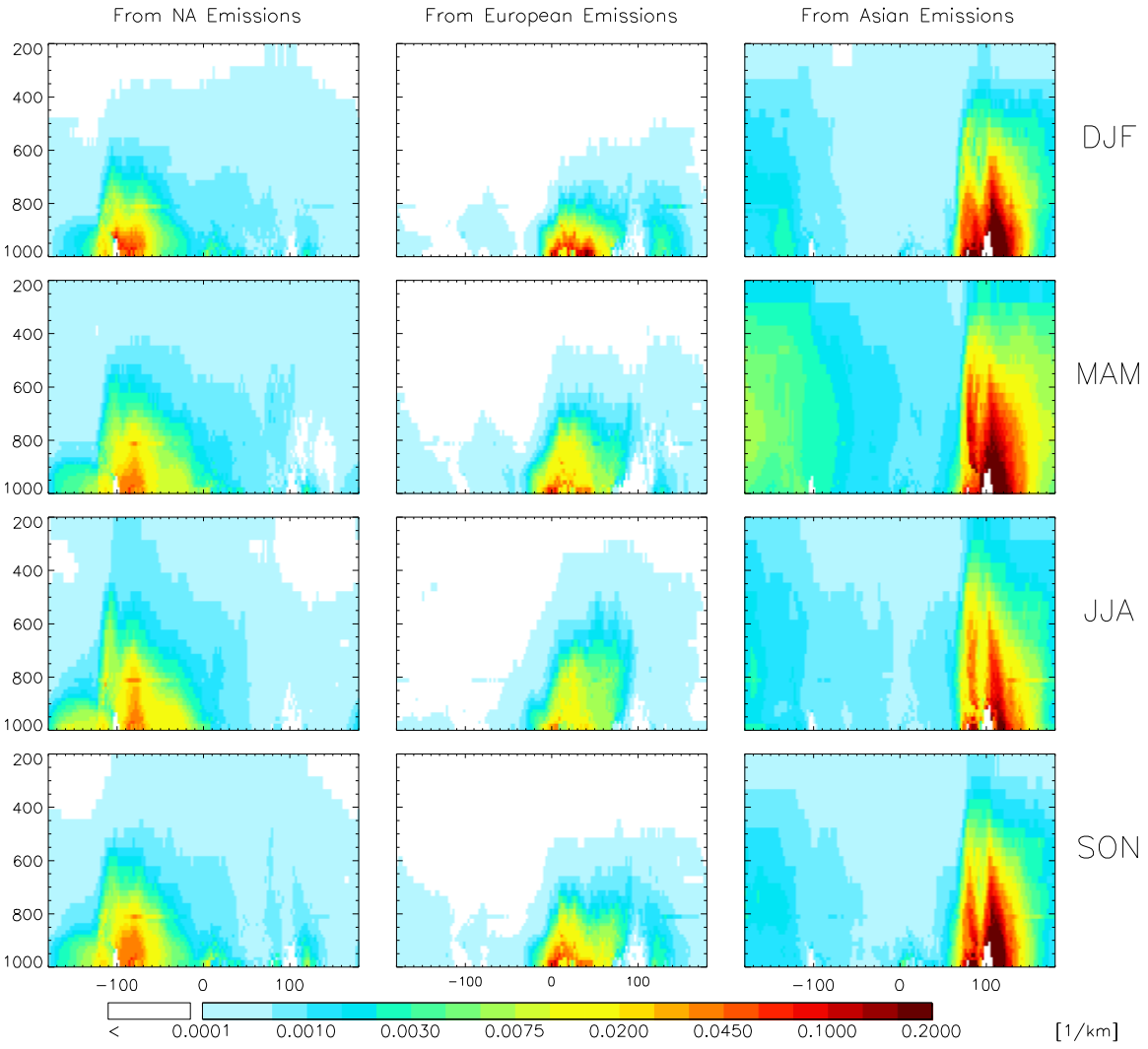

Figure 5.9: Seasonal averages of aerosol extinction due to North American emissions (Column 1), European emissions (Column 2), and Asian emissions (Column 3) averaged from 20-50ºN. Color bar is saturated at a value of 0.2/km. Note the non-uniform scaling of the color bar.

From the vertical distribution of aerosol extinction (Figure 5.9) and CO (Figure 5.10), we see again that lofting occurs most in spring and summer, which are also the seasons for more frequent warm conveyor belts, an important lofting mechanism in East Asia and North America. For all three regions, and both species, winter has the least

lofting, and high concentrations are very localized suggestive of trapping in the boundary layer. In general, lofting is more prevalent over North America and Asia, while most outflow from Europe does appear to remain in the lower troposphere.

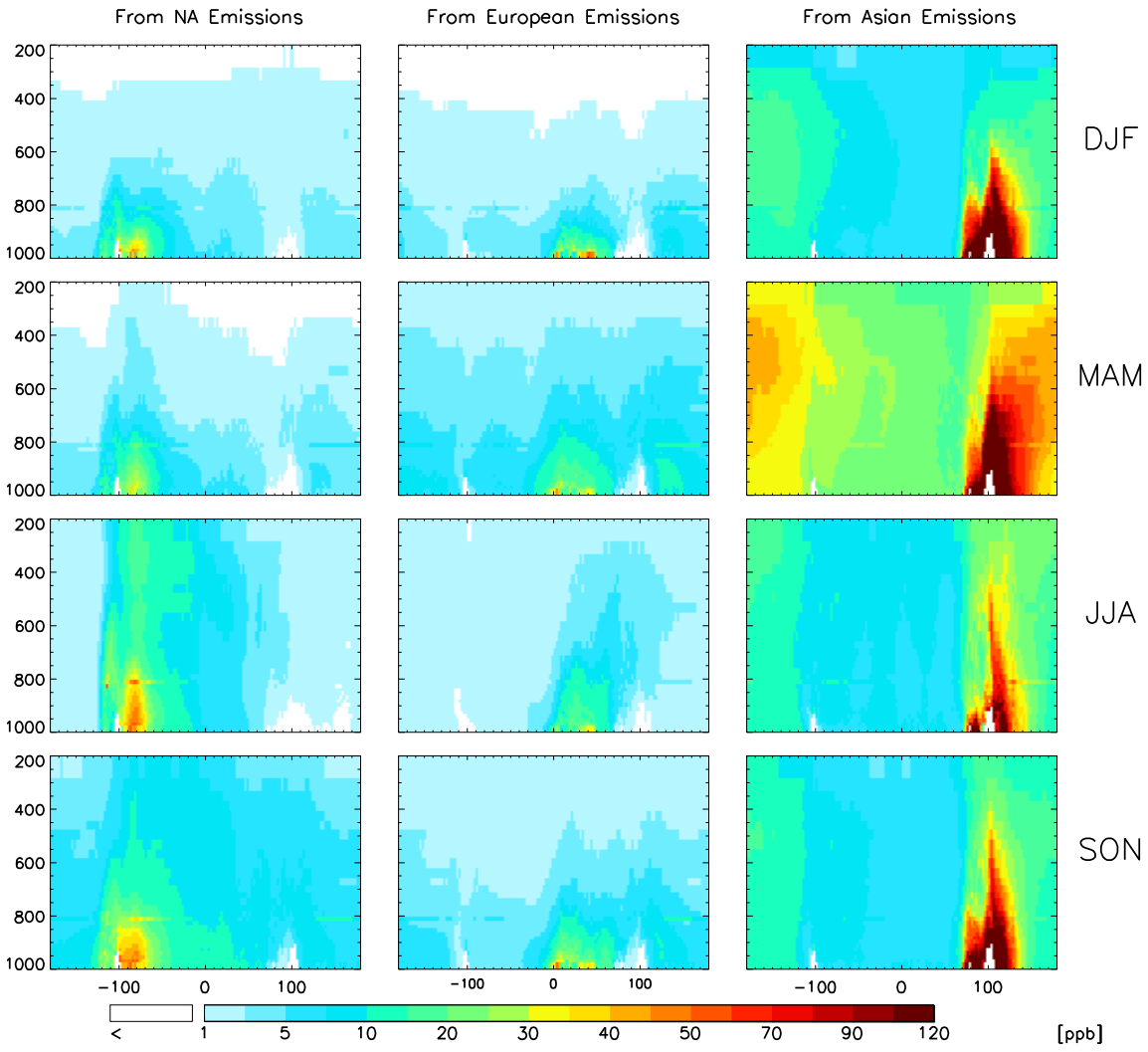

Figure 5.10: Seasonal averages of the vertical distribution of CO (ppb) due to North American emissions (Column 1), European emissions (Column 2), and Asian emissions (Column 3) averaged from 20-50ºN. Color bar is saturated at a value of 120. Note the non-uniform scaling of the color bar.

Europe experiences far fewer warm conveyor belts (Stohl, 2002) and therefore lofting is only slightly higher in summer with increased convection. Summer is also the season where European emissions have the least impact on China. This suggests that

while convection is a useful mechanism for lofting, more of the pollutants are removed due to high summertime OH before being transported to downwind receptor sites.

This contrasts Asia where higher lofting generally leads to a greater downwind impact. Asia has the most vigorous lofting and the greatest hemispheric influence for both pollutant phases. Spring, the season for highest lofting of both CO and aerosols, is also the season where Asian emissions have the greatest impact on the west coast of North America. The larger extinction values and CO concentrations aloft than at the surface of this region downwind (~150ºW) also emphasize the more efficient transport in the free troposphere.

As for species, much as with the spatial distribution, most of the extinction is due to inorganic aerosols, although dust does contribute over Asia. Specifically, in spring we do see that the extinction at the highest altitudes directly over Asia is due to dust, but as it is transported to the west coast of North America, it continues to remain in a higher, more distinct layer (above 700hPa) than the transported inorganic aerosol (above 850hPa). In summer and fall, dust is still emitted, although much less and is not transported much out of Asia.

For North America, we see the source of CO is more localized than in Asia, and that the greater concentrations being exported from the source are in the summer, which also has the highest lofting. However, because of the hydroxyl radical (OH) concentrations and shorter lifetime, CO transport is not as efficient. The greatest influence on the rest of the hemisphere of transport is conversely in fall, when emissions are still high, but CO has a longer lifetime. Contrastingly, aerosols are more efficiently transported in summer, as the enhanced oxidizing capacity would be more beneficial to

the production of sulfate, and according to GEOS-Chem the majority of the lofted and transported aerosol is inorganic aerosol.

These extinction plots also highlight the shorter lifetimes of aerosols by the strong gradients near the source as compared to CO. Transported CO from all regions makes a continual contribution to background concentrations to the rest of the hemisphere. The influence due to transported particulate phase pollutants is more dependent on emissions and transport mechanisms.

From these vertical distributions, we also see the role that topography plays in lofting and subsidence. When looking at emissions from Europe, we see that the mountains in western China lead to orographic lifting of pollutants, but also that subsidence on the eastern side of the mountains aid in bringing high concentrations back to lower altitudes for all seasons except summer, which again could be due to faster removal. This occurs also with the Rocky Mountains in North America, where we see enhanced lofting and then subsidence on the leeward side with Asian emissions.

5.2c Fraction of Pollutants in the Planetary Boundary Layer

Deeter et al., (2007) have shown that the vertical information in CO retrievals generally comes from two regions: the lower troposphere and the middle troposphere. We attempt to exploit the constraints offered by TES on the vertical distribution of CO by examining the fraction of the CO column in these two regions.

To differentiate the lower troposphere, we use daily output planetary boundary layer (PBL) heights from GEOS-Chem coincident with the satellite overpass. We chose to use specific PBL heights rather than a cutoff pressure level in order to better reflect atmospheric distributions and transport mechanisms. PBL heights can also have a strong

impact on the vertical distribution of pollutants and vary with season and location (Lin et al., 2010). Figure 5.11 shows these seasonal and regional dependencies through the seasonal averages of PBL heights from GEOS-5 meteorology used here. Additionally, PBL heights have a strong diurnal cycle, varying by a factor of ~10 from day to night (Lin et al., 2008); for this reason, and the fact that emissions are normally greater during the day (Lin et al., 2010), the following comparisons are made with daytime observations.

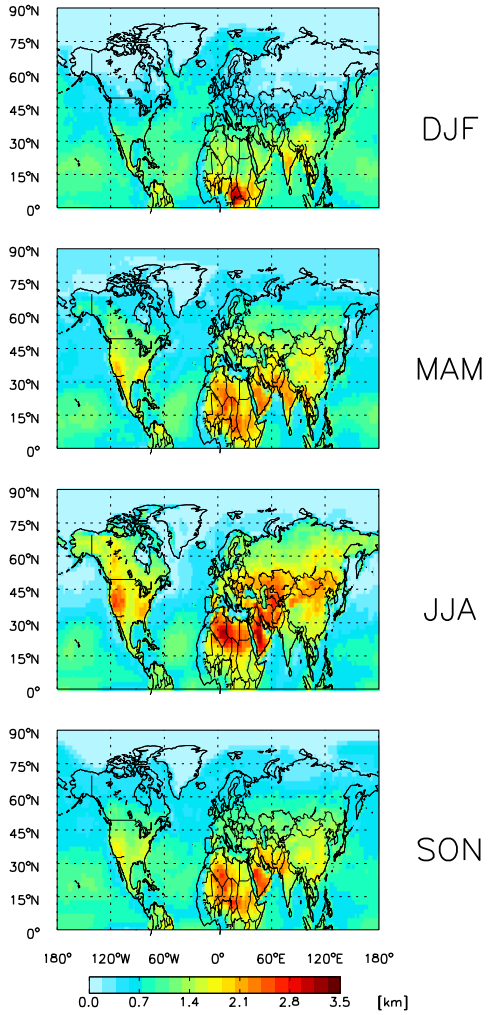

Figure 5.11: Seasonal averages of the height [km] of the PBL in GEOS-Chem.

Seasonal averages of the fraction of the total column CO that are in the PBL as observed by TES and simulated by GEOS-Chem (with the TES retrieval operator) are shown in Figure 5.12. To note, there are some regions where the lowest altitude with a valid observations from TES is above the PBL (over Himalayas and Greenland), fractions therefore cannot be calculated and are disregarded in our seasonal averages. Overall, TES

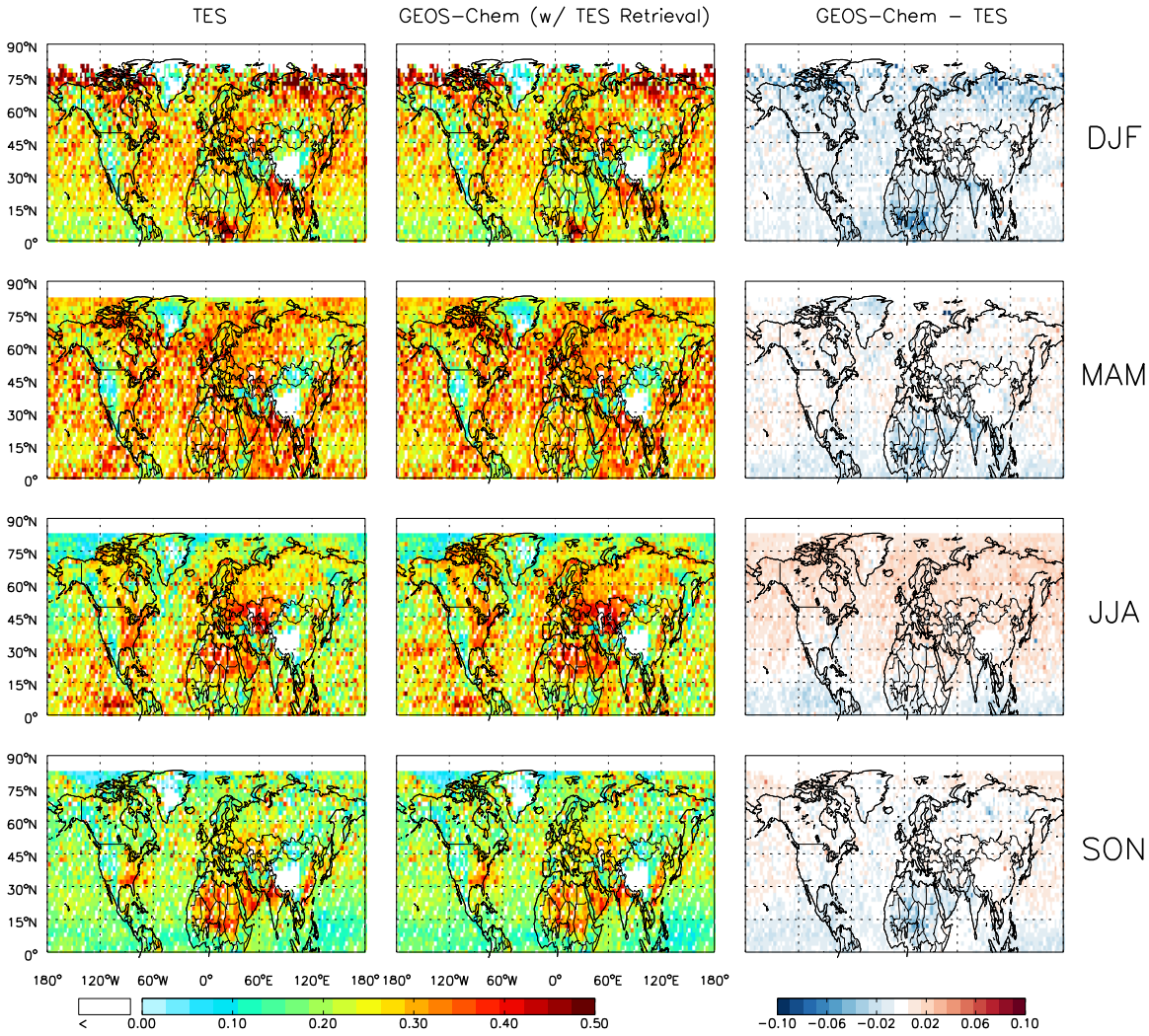

Figure 5.12: Seasonal distributions of the fraction of CO that remains in the PBL as observed by TES and GEOS-Chem (with the TES retrieval operator). Color bar is saturated 0.50.

and GEOS-Chem are in good agreement, although GEOS-Chem shows slightly less CO in the PBL in all seasons but summer, where it shows slightly higher fractions. However, the difference is generally less than 0.05 as shown in Column 3.

This figure also shows the interaction of several factors that determine the amount of CO that remains in the boundary layer: emissions, boundary layer height, lofting mechanisms, and the lifetime of CO. We would assume that near source regions, a greater amount of CO would be in the PBL, such as is evident for fall. However, these source regions are not as evident in other seasons. For example, in spring, values over China and India are much lower, which is most likely due to increased lofting with convection. However, spring is also a season with high lofting off eastern China, but the amount in the PBL is greater than in summer. Part of this can be explained by the PBL heights which are higher in spring, but also the longer lifetime of CO in the winter months. As seen with the total column distributions, CO concentrations build up through the winter months and are often the greatest in spring. With increased emissions in winter and convection also being suppressed, more of the CO emitted will remain in the PBL and increase concentrations. CO concentrations decrease throughout the summer and are the lowest in summer and fall. Fall has the least amount in the PBL which is in large part due to the significantly shallower PBL in GEOS-Chem, but also due to removal throughout the summer and decreases in emissions. Overall, given limitations in the vertical resolution of the observations, these comparisons do not reveal any bias in the simulated vertical profile of CO.

We also contrast these results with fractions of AOD in the PBL. Comparisons between CALIOP and GEOS-Chem fraction of AOD in the PBL are shown in the first

two columns of Figure 5.13 and appear to be completely dissimilar. In almost all of the Northern Hemisphere, CALIOP shows over 70% in the PBL, whereas for GEOS-Chem, fractions are only that high over distinct source regions. Part of this dissimilarity can be explained by the limited instrument sensitivity of CALIOP, which is approximately 2-4 x 10^{-4} $km^{-1}sr^{-1}$, in the troposphere (Yu et al., 2010), reflecting some dependence on assumed aerosol type (by way of the lidar ratio). By assigning clear air observations an

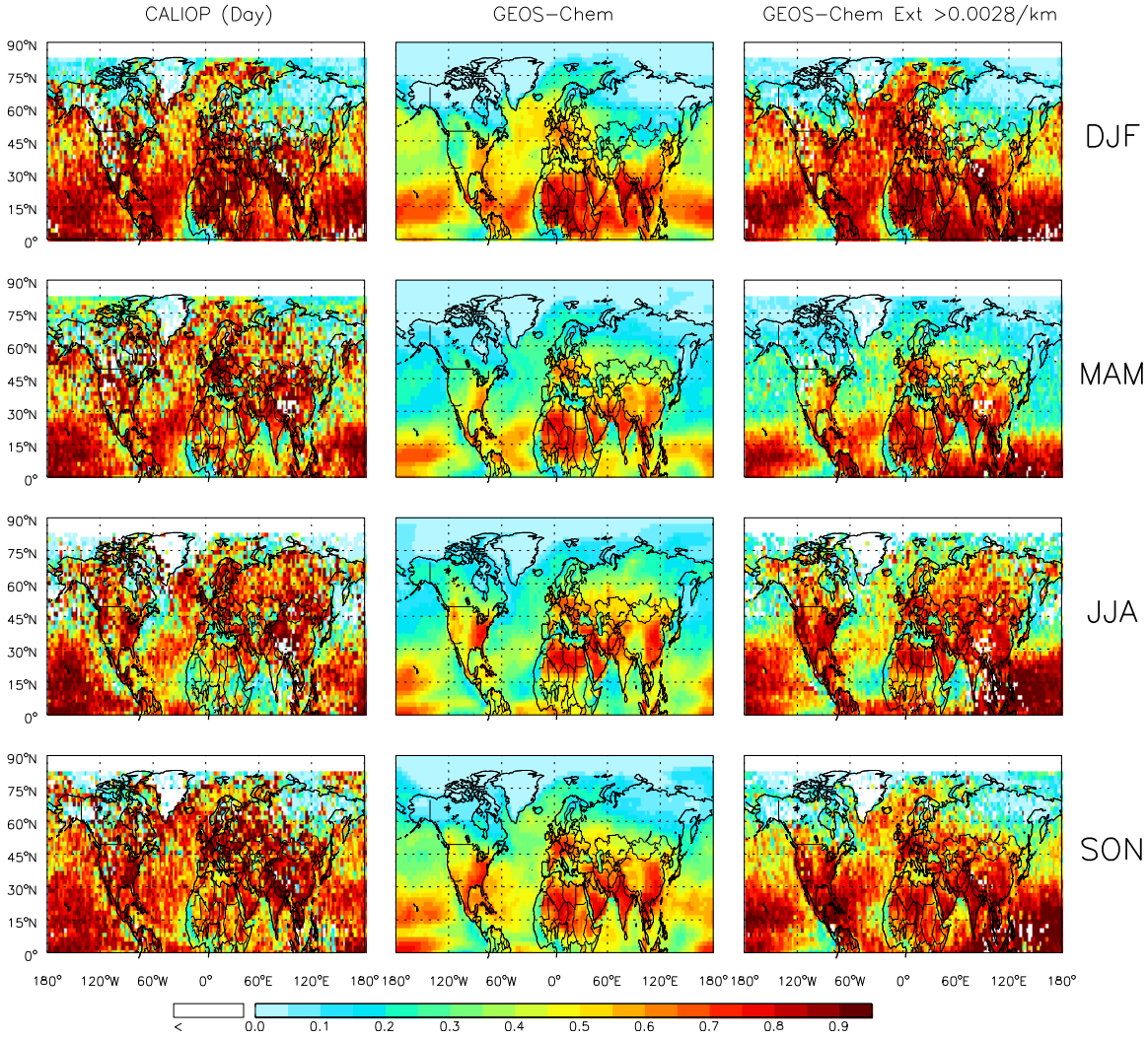

Figure 5.13: Seasonal distributions of the fraction of AOD that remains in the PBL as observed by CALIOP (Column 1) and simulated by GEOS-Chem with all values (Column 2), and eliminating extinction values less than 0.0028 km^{-1} (Column 3).

extinction value of 0km^{-1}, we bias the data low, especially in regions with low loading, such as marine environments and at high altitudes. We explore this by setting a detection limit in GEOS-Chem as well. Since most of the discrepancies are over the ocean, and lidar ratios are smallest for marine aerosol (20±6 sr), we choose to replace extinction values in GEOS-Chem that are less than 0.0028 km^{-1} with a value of 0 km^{-1}. As shown in the third column of Figure 5.13, this improves the comparison with CALIOP. A more exact comparison could be obtained by applying species-dependent detection limits to the GEOS-Chem simulation. We focus here on the spatial patterns in both datasets.

Both CALIOP and GEOS-Chem show high PBL fractions over sources, but those values drop in their outflow region, such as off the east coast of the US and off Asia. This is especially noticeable in spring and summer. The PBL fraction off Asia is also generally lower than off the northeast US, reflecting a greater amount being lofted or more removal in the boundary layer or possibly due to a slightly shallower marine boundary layer.

As with CO, we see some seasonality, although it is much more distinct and does not follow the same pattern. Unlike CO, there are generally higher fractions in winter and lower fractions in spring and summer. We also see that fractions of pollutants in the PBL are generally greater for aerosols compared to CO and with much stronger gradients. Near sources, ~80% of the aerosols are in the boundary layer, but for CO these values are rarely over 50%, again emphasizing the much larger background concentrations of CO that reside in the free troposphere.

The PBL fractions in outflow over the oceans are noticeably different between CALIOP and GEOS-Chem. While a good portion of this is due to the aforementioned issues with instrument sensitivity; even when we apply a detection limit to the model

output, the spatial patterns are still inconsistent, especially during spring and summer, the seasons of the greatest amount of outflow. The gradient in GEOS-Chem is much more noticeable than with the CALIOP observations, again suggestive that GEOS-Chem has either too much lofting near source, such as over Asia, or too much removal of aerosols in boundary layer outflow.

Although these comparisons inform us that the vertical distribution of pollutants simulated by GEOS-Chem does have some general agreement with observations, in order to better investigate the discrepancies, we can compare export from the different source regions using the GEOS-Chem sensitivity simulations.

5.2d Fraction of Pollutants from Tagged Regions in the PBL

Figure 5.14 shows the seasonal average of fraction of AOD that remains in PBL due to each emission region. In conjunction with Figure 5.3, this plot allows us to determine where LRT, as simulated in GEOS-Chem, makes a significant contribution to near-surface air concentrations downwind. This provides insight on how emission reductions (increases) in a source region could potentially improve (degrade) surface air quality in receptor regions.

In order to avoid biasing the distributions of fractions of pollutants in the PBL by columns with very small AOD values, we choose to only include columns where the contribution from the emission region to the total AOD was greater than 0.005. Part of the distributions shown can be explained by the boundary layer heights in Figure 5.11, where a higher boundary layer height will mean more of the atmospheric column is in the

boundary layer and in turn, allows more of the column AOD to be in the boundary layer. This is evident off the southwest and southeast coasts of the US and also explains some of the seasonality.

Nevertheless, when comparing with the tagged column total AODs in Figure 5.3, we also see how particulate pollutants are exported seasonally and regionally in GEOS-Chem. Since particulate pollutants are primarily emitted in the boundary layer, fractions over source regions are generally close to 1. All of the sources that were evident from the

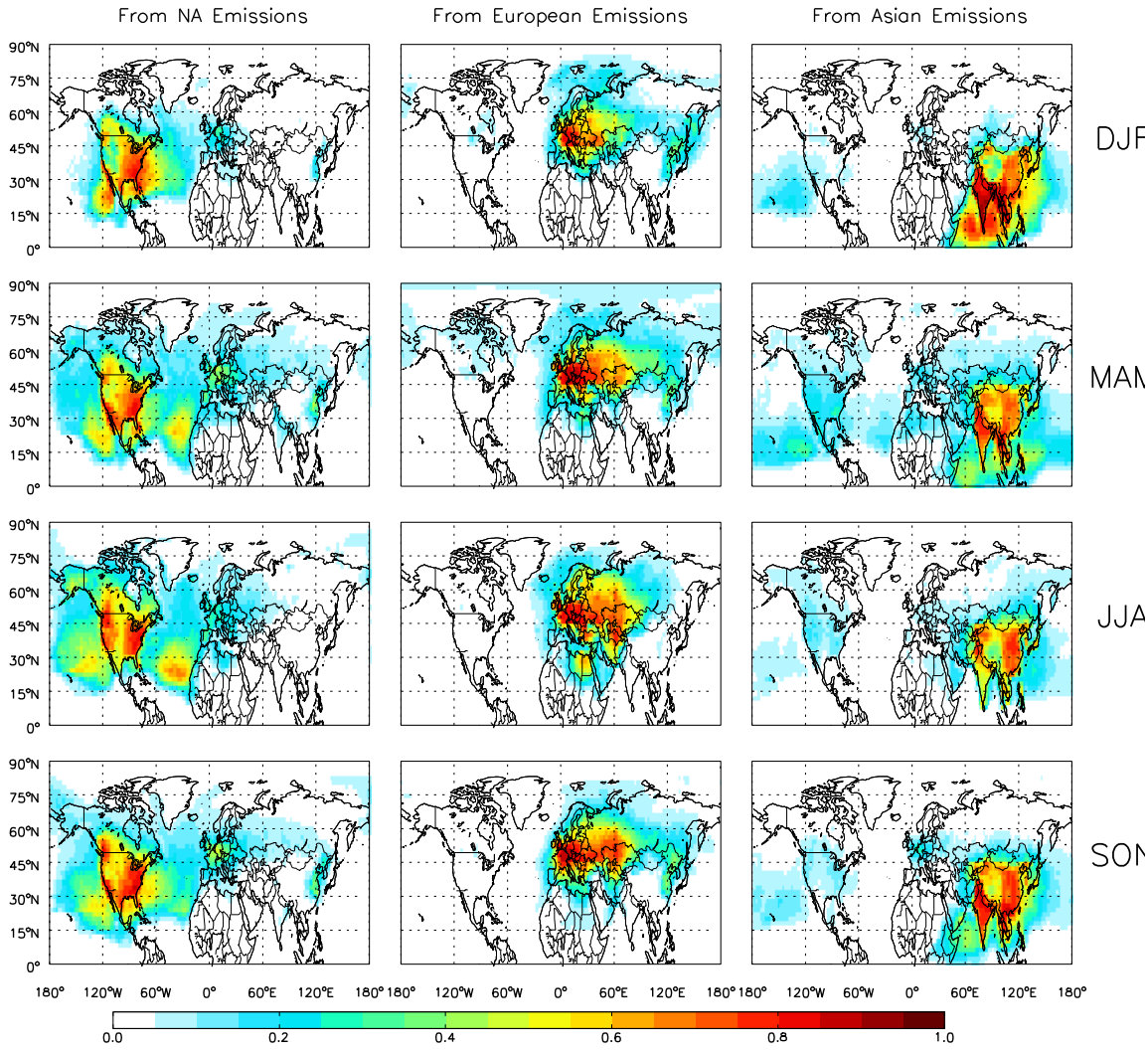

Figure 5.14: Fraction of AOD from each emission region that remains in the PBL as simulated by GEOS-Chem. Locations with AOD less than 0.005 are omitted.

tagged column AOD coincide with regions of high fractions of pollutants in the PBL. There are some slight regional differences; in China, we saw that AOD values are much higher at the source than for European and North American sources. However, the fraction in PBL is lower, especially over the dust source in northwest China and its outflow to Mongolia and eastern China. This agrees with the vertical distributions and Matsuki et al. (2003) who found that because the Tarim Basin is surrounded by high mountains, in order to be transported away from source, dust plumes need to be lofted to above 5 km.

Contrastingly, in outflow regions, which still have high AODs, the fractions are much lower. For example, off the coast of Asia in spring, there are tagged AOD values greater than 0.3, but less than 30% remains in the PBL. Similarly, off the US east coast in summer, the fraction of exported pollutants in the PBL is less than 20%. Europe differs from these regions, in that a much greater fraction of its outflow stays in the PBL. This is especially true for outflow eastward into Asia and to North Africa, while outflow to the North Pole occurs less often in the PBL.

There is also evident seasonality in these distributions as seen from CALIOP and the total column simulated by GEOS-Chem (as previously discussed with Figure 5.1), where fractions in the boundary layer are generally higher in fall and winter and lower in spring and summer. This is true for both source and outflow regions. Again, this is partly due to the seasonality in PBL heights which are also generally lower in fall and winter, but also lofting occurs less in fall and winter when convection is not as prominent.

These distributions also highlight the efficiency of free tropospheric transport over boundary layer outflow in GEOS-Chem. In spring, when lofting is more prominent,

exported pollutants will have a greater impact downwind; however, the majority of this contribution is at higher altitudes, depicted by the low fractions in the PBL (less than 40%) seen at all downwind sites. Europe again is the only exception, where many downwind sites still have large PBL fractions. Yet, the overall contribution to the AOD is very small.

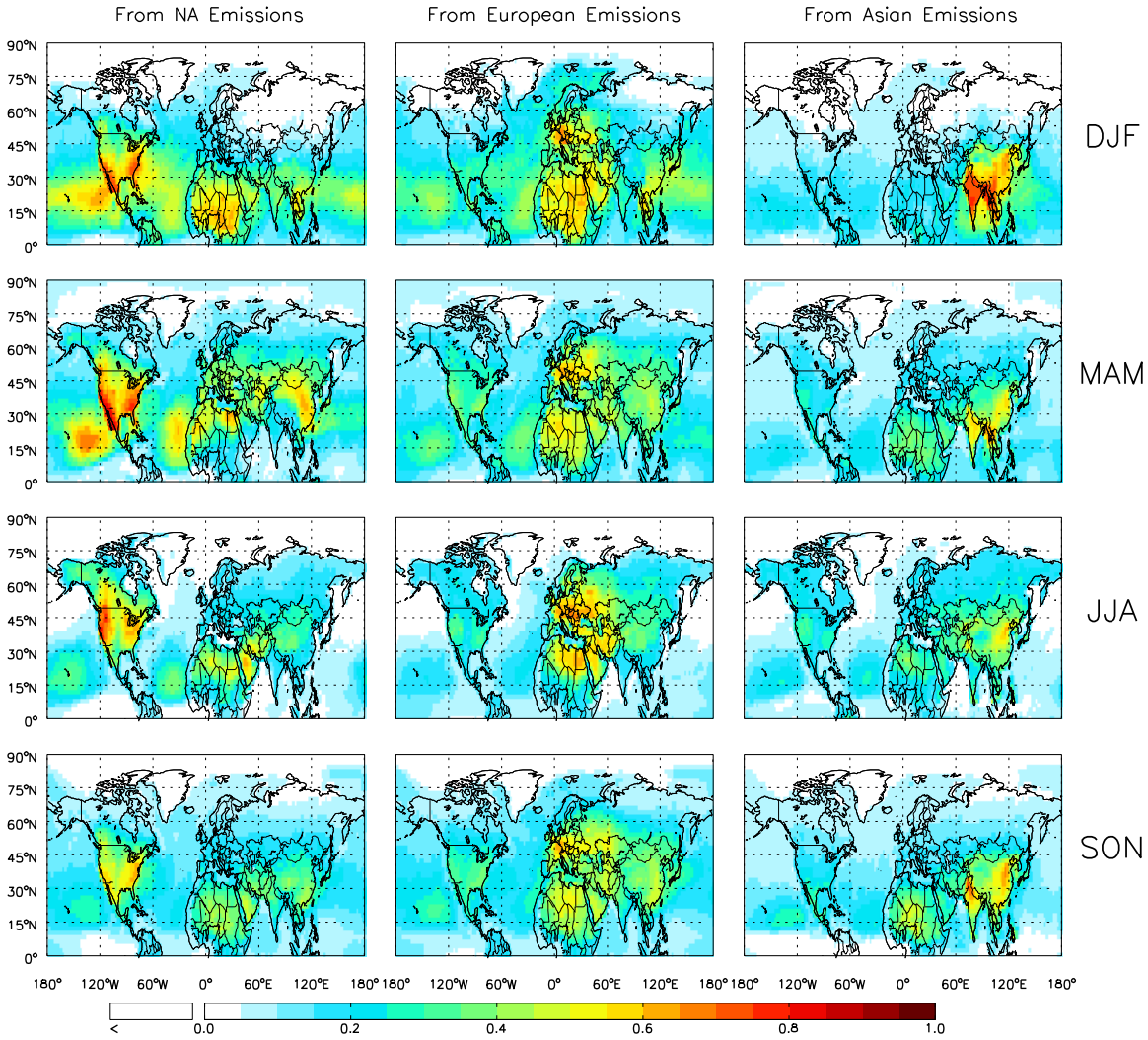

Figure 5.15: As for Figure 5.14 but for CO. Locations with less than 1.0×10^{13} molecules/cm² are omitted. Colorbar is saturated at 1.0×10^{18} molecules/cm².

These comparisons with CO, also highlight difference in the way particulates and gas phase pollutants are exported. Near sources, aerosol PBL fractions are higher than

CO PBL fractions (Figure 5.15), depicting that there is both possibly more lofting with CO as well as a longer lived free tropospheric background of CO. The spatial gradient in these fractions is much steeper for aerosols, showing that the concentration of aerosol that remains in the boundary layer disappears more quickly than for CO, which suggests much faster removal of particulates over the gas phase in the boundary layer. This also highlights the necessity of particulate pollutants to be lofted into the free troposphere in order to be efficiently transported, along with the fact that most downwind impacts of particulate pollutants are not at the surface but in lofted layers.

We also see differences in the vertical height at which pollutants from different regions are exported. For North America, the fractions of CO in the PBL off the southwest coast are notably higher than off the northeast coast. In the northeast, the primary mechanism for export is by warm conveyor belts that quickly loft species. On the southwest coast, however, outflow is generally with the low level offshore winds.

Additionally, northeast China has a greater fraction of CO in the boundary layer than southeast China, even though Figure 5.6 had shown them both to be regions of high column totals. This is in agreement with the fraction of the total column of CO in the PBL (Figure 5.12). This could be due to advection with the mean wind supporting low level outflow, since the wind in northeast China is more predominantly westerly, and more northerly/northeasterly in south east China.

For Europe, boundary layer outflow of CO dominates, especially southwards towards Africa. Compared to Asia, in general, a higher fraction of CO outflow remains at lower altitudes, even though the overall concentrations might be lower. Boundary layer

transport of aerosols is not as evident as with CO. As with North America and Asia, most aerosol transport occurs when pollutants are lofted out of the PBL.

5.3 Regional Profiles

The previous sections have made regional comparisons on a hemispheric scale, but we also want to specifically examine export and transport from these three regions. For each of the regions, we choose a source area and compare the average extinction profile to a downwind region for spring, a season with heightened export. These regions are shown in Figure 5.16.

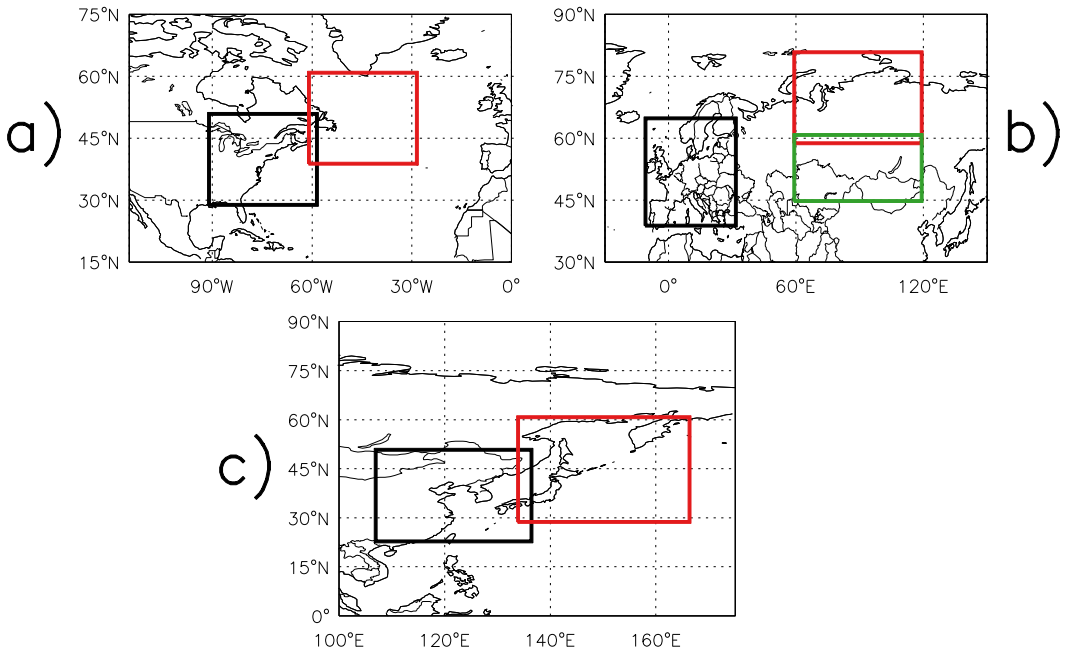

Figure 5.16: Grid boxes used for regional averages for (a) North America, (b) Europe, and (c) Asia. Source regions are outlined in black and outflow regions are in red and green.

5.3a North America

For North America, the average extinction profile observed by CALIOP is similar in the export region and the downwind site (Figure 5.17a). This contrasts GEOS-Chem

which shows much less at the downwind site than at the source. At the source, although the profile shapes are similar, CALIOP is greater than GEOS-Chem in the lower atmosphere, while GEOS-Chem is slightly greater above 750hPa. This could suggest that GEOS-Chem is not showing as much low level outflow, which could explain the

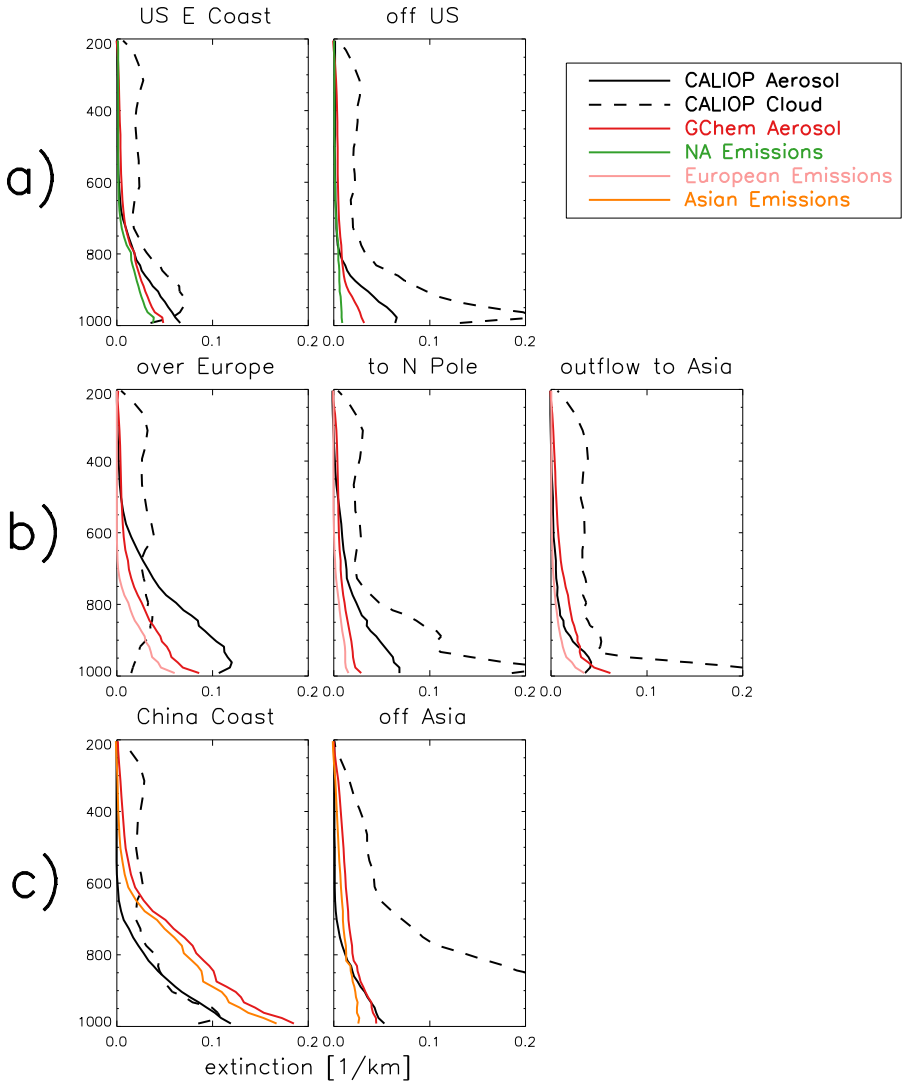

Figure 5.17: Average spring 2007 extinction profiles for boxed regions (with corresponding letters in Figure 5.16) of CALIOP aerosol extinction (solid black), CALIOP cloud extinction (dashed black), GEOS-Chem aerosol extinction (solid red), and aerosol extinction from NA emissions (solid green), European emissions (solid pink), and Asian emissions (solid orange).

difference downwind. It is also noticeable that the tagged emissions from North America make a negligible contribution to simulated extinction near the surface downwind, suggesting that particulates are being quickly removed. The contribution from North American emissions, however, accounts for almost all of the extinction aloft, indicating that pollutants in the boundary layer are removed proportionally faster than pollutants lofted into the free troposphere.

The cloud profiles from CALIOP show clouds throughout the column at both the source and the downwind site. However, at the downwind site, these clouds are concentrated at a lower altitude. The comparatively higher level clouds at the source could suggest convection and lofting of the pollutants. Additionally, as previously mentioned, the CALIOP cloud and detection algorithm often has difficulties in outflow regions where the two are mixed, which could mean that some of these discrepancies could be due to misclassification in the CALIOP retrieval.

5.3b Europe

Profiles of extinction over Europe (Figure 5.17b) are higher than over North America, but this is most likely due to the grid box choice for North America which included more marine atmosphere than over Europe. Profiles from GEOS-Chem have a similar shape to those from North America; however, the profile from CALIOP suggests extinction values remain higher above the surface. Similar to North America, aerosol extinction from CALIOP is higher at lower altitudes, while GEOS-Chem is greater at higher altitudes, suggesting that GEOS-Chem might have too much lofting over Europe, but could also be due to the low detection limit of CALIOP missing elevated aerosol layers with low concentrations. GEOS-Chem also simulates significantly lower extinction

values in the outflow to the North Pole than observed by CALIOP, especially at lower altitudes. Contrastingly, in outflow to Asia, GEOS-Chem is higher than observed by CALIOP throughout most of the profile and especially at the surface. This could suggest too many pollutants are simulated in GEOS-Chem or some vertical misplacement, but this is difficult to determine because of the scarcity of valid profiles from CALIOP in these outflow areas (as shown in the spatial distributions of Figure 5.1).

5.3c Asia

Unlike Europe and North America, GEOS-Chem is significantly higher over Asia than observed by CALIOP, both near the surface and aloft (Figure 5.17c). Extinction values are also overall higher than the other two regions. However, in the outflow region off Asia, the extinction profile from GEOS-Chem is also significantly lower than observed by CALIOP at lower altitudes, again possibly suggesting that there is too much removal of pollutants in the low level outflow. At higher altitudes, they are in relatively good agreement, showing higher values aloft than in the outflow regions of both Europe and North America.

Additionally, the cloud profiles suggest higher or thicker clouds aloft than the other regions, supporting that Asia has more rigorous convection, enabling it to more efficiently loft pollutants to be exported. These high extinction values for clouds could also suggest that a misclassification in the cloud detection could bias these comparisons.

6 Temporal Variability of Transport in the Northern Hemisphere

While the seasonal perspective of Chapter 5 gives us a good sense of what transport looks like on average, it does not tell us about the frequency or magnitude of events in each region. Again, due to many of the previously mentioned sampling issues, we cannot effectively analyze each event separately, but we choose to investigate the regularity and scale of transport events for spring 2007 by looking at time series of column AOD and CO for each emission region. We choose to focus on spring as it is the season with the most transport of both CO and particulate pollutants to downwind sites for all regions.

6.1 Regional Time Series Comparisons

6.1a North America

Pollutants are mainly exported out of North America from the eastern US and transported across the North Atlantic to Europe. To examine the export out of the eastern US, we look at the time series for the source region and for an area downwind (same averaging boxes as Figure 5.16). In the time series of AOD observed by CALIOP and simulated by GEOS-Chem, there are several days that highlight periods of increased export from the source (Figure 6.1a). For this comparison, we designate a day with increased export as having a column AOD greater than the mean plus one standard deviation for that season. In general, these time series points are an average of 10 grid boxes. For CALIOP, these grid boxes are an average computed from approximately 20

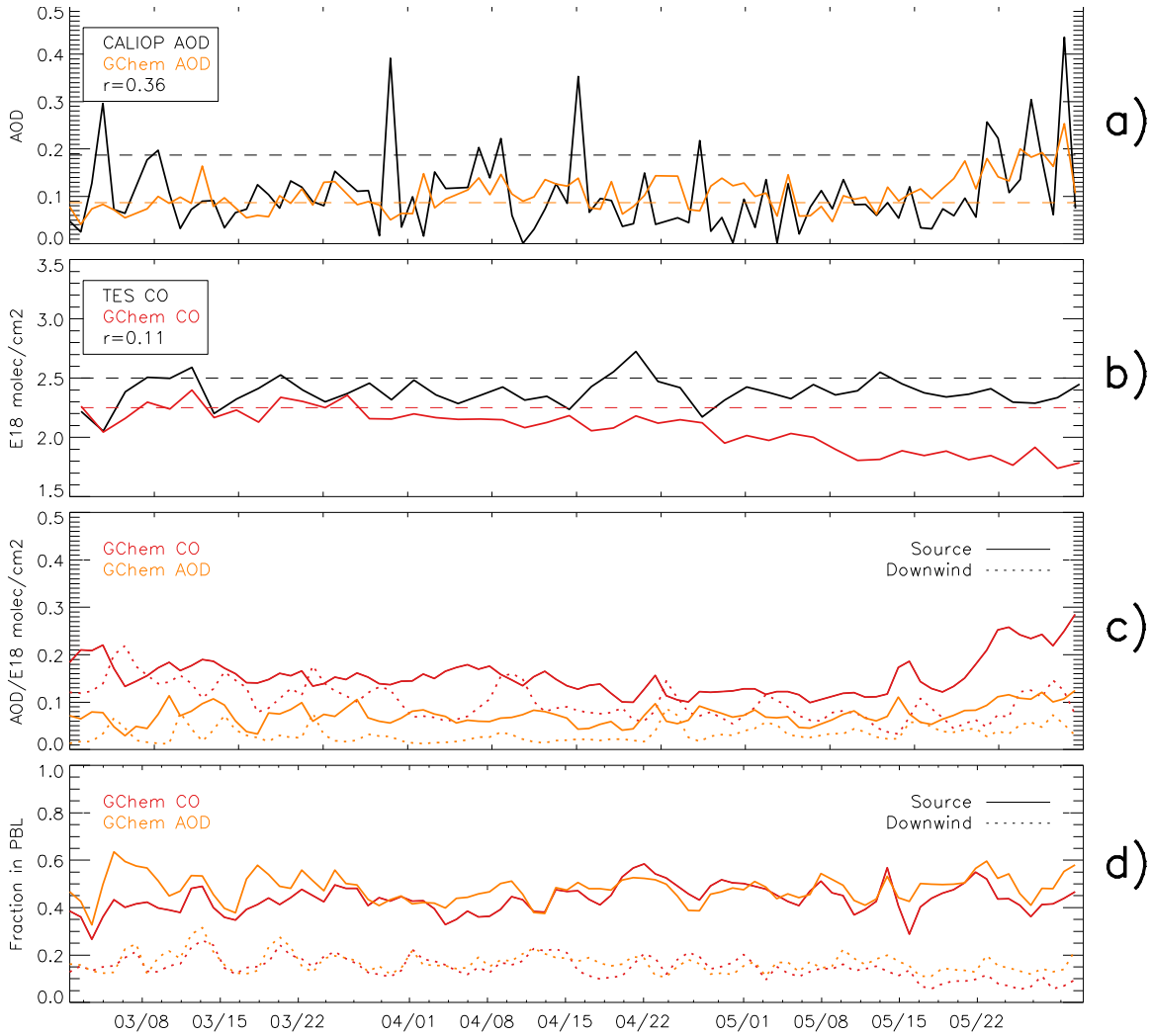

Figure 6.1: Time Series of (a) AOD at the source region observed by CALIOP (black) and GEOS-Chem (orange), dashed line is for mean plus one standard deviation; (b) CO column concentration at the source region from TES (black) and GEOS-Chem (red); (c) tagged AOD (orange) and CO (red) from GEOS-Chem at the source and downwind; and (d) fraction in the PBL of tagged CO and AOD at the source and downwind.

observations (as discussed with Figure 2.4). It is important to again emphasize here, that due to the sampling period of CALIOP, these points in the time series are not representative of the whole averaging box but only the area over which the satellite passed for that day. Figure 6.2 shows where CALIOP made valid observations for March

1-16th (because CALIOP has a repeat orbit of 16 days) and illustrates how this smaller sampling size can make these comparisons more difficult.

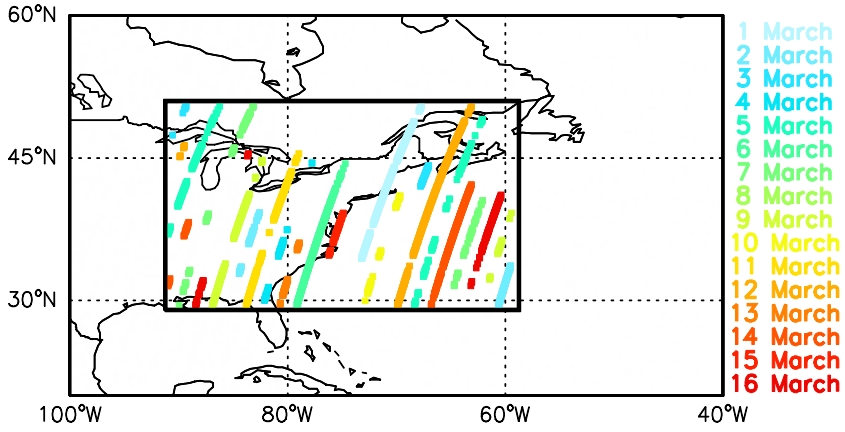

Figure 6.2: CALIOP valid observations over the North American export region averaging box (black box) for the time period of March 1 through March 16, 2007.

For spring 2007, we find that, although CALIOP has a slightly higher mean AOD, GEOS-Chem simulates the same number of days with high export as CALIOP (11). However, these days do not coincide, and the model only captures 13% of the variability in the AOD export from North America observed by CALIOP. In general, we would expect CALIOP to have more variability compared to GEOS-Chem because again CALIOP AOD values that go into these averages are over a small portion of a GEOS-Chem grid box rather than an average for the whole area in the 2º by 2.5º grid box.

GEOS-Chem simulates fewer days where the column concentration of CO is substantially over the mean (Figure 6.1b), with only seven days that meet the criteria for high export. This is to be expected due to the high background concentrations of CO, which makes using column concentrations to differentiate days with greater export more challenging. While TES observations, as previously noted, are generally higher than

simulated by GEOS-Chem, only six days can be considered as having increased export of CO. The correlation between TES and GEOS-Chem CO is much smaller than CALIOP and GEOS-Chem AOD at the source region (r=0.11).

Away from the source, TES and GEOS-Chem have a slightly higher, albeit negative, correlation coefficient (r=-0.2, time series not shown). These negative values could suggest transport error which would cause events to be out of phase. Conversely, the correlation between CALIOP and GEOS-Chem AOD is significantly reduced (r=0.04).

We also use the time series to investigate whether CO and aerosols are co-transported during LRT events. The correlation between CO and aerosols in the source region is low, but similar, for both the observations and the simulation. For TES CO and CALIOP AOD the correlation coefficient is -0.33, while the simulated AOD and column CO (with the TES retrieval operator) from GEOS-Chem is -0.34.

Away from sources, the model retains the correlation between CO and aerosols (r=-0.31), however, this correspondence is significantly reduced (r=0.03) in the TES and CALIOP observations. These negative values are possibly the result of the fact that AOD values in these regions are largely due to sulfate, which is primarily the result of oxidation of sulfur dioxide rather than direct emission, whereas CO can be emitted directly. Additionally, CO values contain large background concentrations, and therefore these comparisons are not effectively comparing rather events occur simultaneously.

We examine these differences through the time series of tagged emissions and fractions in the PBL simulated by GEOS-Chem (Figure 6.1c and d). From the sensitivity run, we find that there are several more days where the AOD and CO from tagged North

American emissions meets our requirements for increased export (16 for AOD and 12 for CO). This difference is to be expected as the sensitivity simulation removes dampening of results by background concentrations. This is further supported by the finding that tagged CO and AOD in the export region are more highly correlated (r=0.67) than the total column concentrations, which implies that CO and AOD have some similar, but not identical, sources and export mechanisms. This is additionally seen by the fraction of tagged emissions in the PBL. While the mean fractions of tagged CO and contribution to AOD in the PBL are similar (0.44 and 0.48, respectively), the correlation is only moderate (r=0.52).

Downwind, mean fractions in the PBL for both species are lower (0.15 for CO and 0.17 for AOD), suggesting that pollutants are more concentrated aloft (partially due to a shallow marine PBL). The correlation between concentrations of tagged CO and tagged AOD decreases downwind (r=0.42), most likely due to the fact that particulates are being removed more quickly than CO. However, the correlation between the two for fractions in the PBL increases downwind (r=0.64).

This could explain the discrepancy between observation and model correlations at the downwind site, where GEOS-Chem shows that AOD and CO are better correlated than observed. From the lower fractions in the PBL downwind, GEOS-Chem could be suggesting that high AOD and CO events are primarily due to lofted layers.

6.1b Europe

Unlike North America, GEOS-Chem not only simulates a higher mean AOD in the export region of Europe, it also simulates several more high AOD events at the source than observed by CALIOP (14 and 9, respectively). Conversely, GEOS-Chem shows

fewer high AOD events in both the downwind regions than CALIOP (13, 15). This could suggest that GEOS-Chem may be exporting too many particulate pollutants from Europe, but underestimating transport downwind. This is further substantiated by the fact that CALIOP and GEOS-Chem are better correlated in regions close to source (r=0.33 over Europe and r=0.40 for outflow to Asia), and less correlated further downwind (r=-0.08 for outflow to the North Pole). This does not hold true for CO, where the correlation coefficients between TES and GEOS-Chem are similar for all regions, but slightly higher away from sources (r values of 0.57 for source, 0.64 for North Pole, and 0.61 for outflow to Asia).

The correlations between TES CO and CALIOP AOD for all regions of export/ are low (r values of -0.04 for source, -0.02 for North Pole, and 0.15 for outflow to Asia). However, GEOS-Chem simulates the correlation for AOD and CO in outflow to the North Pole to be much higher (r=0.44), where the model transports most of the CO and aerosols above the boundary layer. This can suggest that GEOS-Chem over-emphasizes transport of particulates aloft.

6.1c Asia

As with North America and Europe, correlations between CALIOP AOD and GEOS-Chem are better near the source (r=0.41) than in the outflow region (r=0.05); while correlations between the time series of CO simulated by GEOS-Chem and observed by TES are better away from the source (r=0.74 compared to r=0.66 near the source). Again, this could partly be due to the vertical distribution, as correlations for fraction in the PBL follow the same pattern. GEOS-Chem and TES CO fraction in the PBL have an r=0.96 at the source and an r=0.99 downwind, while GEOS-Chem and

CALIOP AOD fraction in the PBL have a higher correlation (r=0.64) at the source than downwind (r=0.47).

6.1d Summary of Regions

Most of the correlations discussed here, were very low. We want to re-emphasize the discussion of Chapter 3 on sampling issues, by restating that these sampled time series might miss a transport event or over-emphasize an event due to a slight misplacement in time or space; and that in general, any comparison of model simulations with satellite observations with no cross-track scanning is going to be particularly susceptible to model transport errors.

That being said, what we can glean from these times series is that pollutants are being exported continually from these three source regions throughout the spring season with a few well-pronounced events. In general, GEOS-Chem favors export above the PBL, except for outflow from Europe to Asia. CO is lofted out of the PBL more than particulate pollutants, except over the US east coast. Because CO is spread throughout more of the atmospheric column, when outflow occurs in the free troposphere, the vertical placement of CO and AOD in downwind regions is more similar than with boundary layer outflow which reflects differences in lifetimes.

Additionally, we find that, with the exception of North America, GEOS-Chem captures more of the variability observed in CO than for AOD. The model also reproduces more of the variability in AOD observed by CALIOP near the source than at the downwind site, which is opposite to CO, where GEOS-Chem is more highly correlated with TES observations away from the source.

6.2 IMPROVE Time Series

In order to determine the potential surface impact of Asian emissions on the northwestern coast of North America, we also looked at spring 2007 time series of sulfate concentrations at two IMPROVE sites and compared them with concentrations simulated by GEOS-Chem sampled for the same grid box (Figure 6.2). The White Pass (WP) site is at a higher elevation (1827 m) and should therefore be more frequently influenced by elevated layers transported from Asia, whereas Mount Rainier (MR) at 439 m would potentially be more influenced by local emissions. This is simulated in the model where we see that the time series of total sulfate concentration at White Pass is highly influenced by the contribution from Asian emissions (r=0.9), but Asian emissions do not dominate the variability in sulfate concentrations at Mount Rainier to the same extent (r=0.65). In general, the model predicts that Asian emissions make up ~50% of the total sulfate concentration at White Pass and ~25% at Mount Rainier. We also see that the model simulates several locally driven enhancements throughout the season with very little contribution from Asian emissions (May 27th for example).

GEOS-Chem is able to capture many of the enhancements noted in the IMPROVE data, such as on March 31st and April 27th. The model does overestimate concentrations, especially during March, for both sites. Overall, the model captures more of the variability at the IMPROVE Mount Rainier site (r=0.55) than for White Pass

(0.46). This may suggest that accurately simulating LRT impacts is more challenging than local emission influences.

For both the model and the IMPROVE sites, the Mount Rainier location generally shows higher concentrations than at the White Pass site. Sulfate concentrations at Mt. Rainier and White Pass are highly correlated in the observation (r=0.78), but this is not reproduced in the model (r=0.12).

In order to test the assumption that transported air masses would first reach high altitude sites and then subside to lower altitudes, we also looked at lag (using preceding or proceeding observation) correlations between observations. For the IMPROVE sites, the correlation for a lag of +1 for Mount Rainier was low 0.29. By contrast, the +1 lag correlation for White Pass was 0.61, suggesting that there is better correlation when we consider that air masses arrive at the lower altitude site before the high altitude sites, which could be suggestive of boundary layer flow forced orographically as it moves inland.

However, air masses should only take a day to subside and IMPROVE measurements are only taken every third day, so a lag correlation of 1 would suggest that it took three days to subside or three days to rise. We investigate this further by looking at the full daily time series of sulfate concentrations from GEOS-Chem (Figure 6.3) rather than the sampled every three day concentrations. Here we see that many events where it appeared that GEOS-Chem was suggesting that high altitude enhancements were preceded by a low altitude enhancement (such as April 27th and 30th), are the result of sampling out periods of transport events, such as the high peak on April 29th. With the

full time series, we also note that the simulated +1 lag correlation for tagged Asian emissions at Mount Rainier increases to 0.77 from 0.09 for the sampled time series.

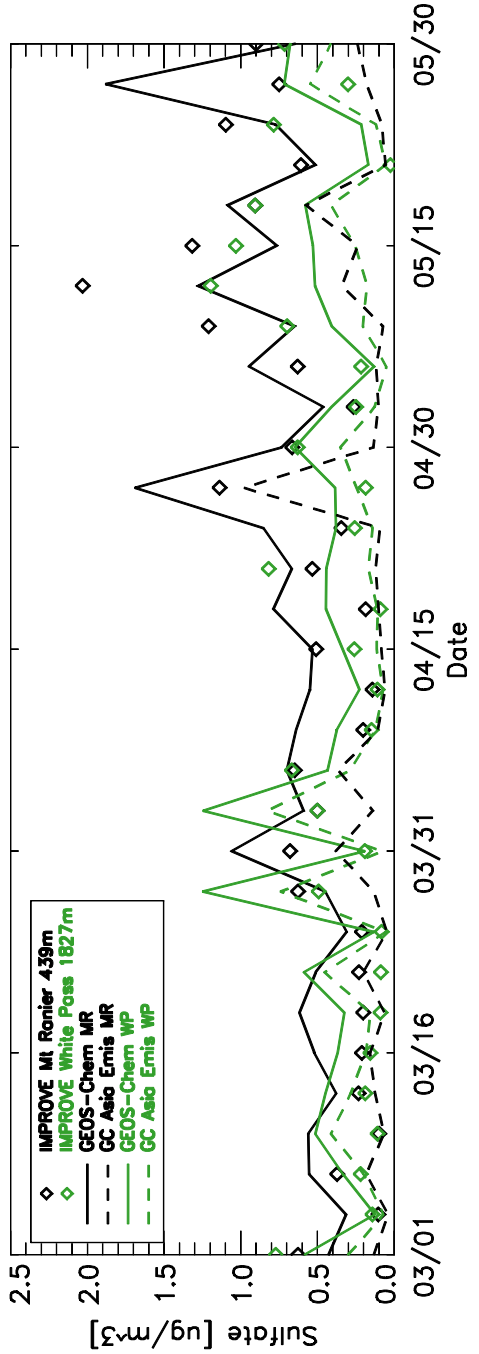

Figure 6.4: Spring 2007 Time Series of Sulfate Concentrations measured at the Mount Rainier IMPROVE site (black diamond), White Pass site (green diamond), simulated for the Mt Rainier (solid black line) and White Pass (solid green line) grid boxes by GEOS-Chem, and due to Asian emissions (dashed line) in GEOS-Chem.

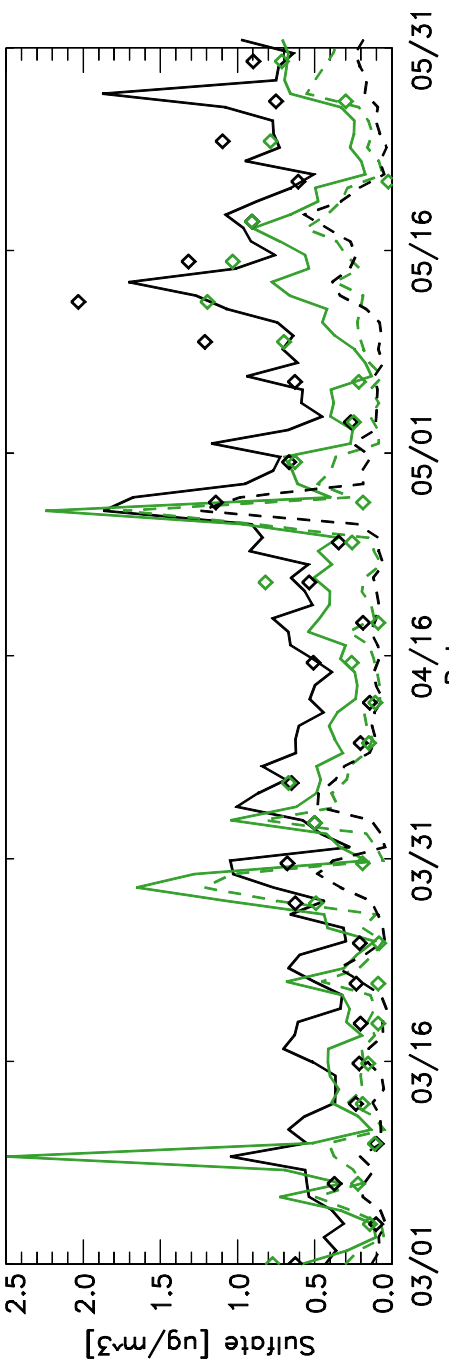

Figure 6.5: Same as for Figure 6.4 but with GEOS-Chem concentrations for all days.

To confirm that plumes were actually descending in the model, we also looked at the vertical profiles of extinction for these events as in Figure 6.4 which shows a lofted plume as it traverses the North Pacific and subsides over the northwest coast of the US.

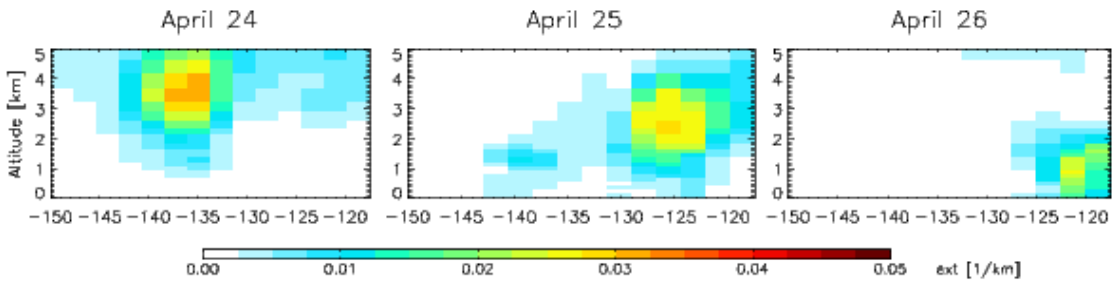

Figure 6.6: Vertical distribution of extinction from Asian emissions as simulated by GEOS-Chem for April 24th -26th, 2007 averaged from 44-48ºN along the latitudes 150-117.25ºW.

These comparisons between GEOS-Chem and IMPROVE could suggest that that concentrations at both sites are primarily driven by local emissions with less influence from foreign air masses than simulated by GEOS-Chem. However, as previously mentioned with the satellite observations, although there is some agreement between GEOS-Chem and the IMPROVE sites on specific enhancement events, the data suggests that observations with poor temporal resolution are unable to fully resolve transport events and make it especially difficult to determine transport and subsidence mechanisms.

7 Summary and Future Work

7.1 Summary

The goal of this work was to use A-Train satellite observations in conjunction with the GEOS-Chem model to analyze the vertical distribution of pollutants during export and long range transport in the Northern Hemisphere. We used CO measurements from TES, AOD and extinction values from CALIOP, and AOD from MODIS in order to analyze gas and particulate phase pollutants for the period of December 2006-November 2007.

While the original goal of this work was to analyze distributions during individual transport events, initial analysis showed that the interference of clouds, the small footprint of satellite observations, and the distance between scans constrained our ability to track plumes as they progress on short time scales. However, it was also shown that these sampling issues had a much smaller impact on seasonal scales. We therefore focused our analysis on seasonal averages of long range transport.

The model and satellite observations both show that pollutants are being continually exported from the main source regions in the Northern Hemisphere with several particularly high LRT events in spring and summer. The model reproduces the spatial distribution of pollutants in the Northern Hemisphere, capturing observed source regions of CO and particulate pollutants and their seasonal variability. For both CO and aerosols, major source regions for all seasons include eastern China, the eastern US,

western Europe, and western Africa. However, export from these regions is generally most evident in spring. While GEOS-Chem has an overall low bias in CO to TES; for aerosols, disagreement mainly arises in outflow over oceans, where GEOS-Chem noticeably underestimates AOD in comparison to both MODIS and CALIOP.

This discrepancy was further examined through vertical distributions of CO and aerosol extinction. It is generally understood that pollutants are more efficiently transported in the free troposphere where they are subject to less removal and stronger winds. This behavior is captured by GEOS-Chem. No bias is apparent in the vertical distribution of CO simulated by the model; however, the limited vertical sensitivity of IR satellite observations limits our ability to test the GEOS-Chem simulation of CO. The lidar observations of aerosols from CALIOP provide an unprecedented degree of vertical resolution. While the model captures the particulate source regions identified by CALIOP and MODIS, it overestimates the concentrations of aerosol pollutants and lofting over Asia and Europe. Conversely, GEOS-Chem underestimates aerosol extinction in outflow regions across the Northern Hemisphere compared to CALIOP. This indicates that boundary layer outflow of aerosols may be more common than simulated by the model and removal processes in the boundary layer are possibly too efficient.

There are also noted differences between the vertical distribution of CO and aerosols that give some indication of how the different phases are transported. Aerosols are concentrated more at lower altitudes near sources, while CO is distributed throughout the column. The high background concentrations of CO, due to its longer lifetime, make identifying transported plumes more difficult but also make the downwind impact greater than for aerosols. Furthermore, the relative insolubility of CO limits the efficiency of

removal processes in the boundary layer which are removing particulate pollutants too quickly. Further downwind, we see greater concentrations of transported CO in the PBL than for aerosols.

We also used two IMPROVE sites: White Pass, with an elevation of 1827 m, and Mount Rainier at 429 m, in order to infer the downwind impact of transported plumes simulated in GEOS-Chem at different altitudes. For the surface observations, there is some variation in the concentrations at the two sites, possibly suggesting different air mass influences or transport mechanisms. However, the inability to track the progression of plumes and the course temporal resolution makes it difficult to conclusively validate the ability of GEOS-Chem to simulate these transported plumes and differentiate the altitude-dependent impact and transport mechanism of plumes from local emission sources on a receptor site.

7.2 Future Work

The outcome of this work was to locate specific regions of disagreements between satellite observations and model simulations with regards to the vertical distribution of pollutants as they were exported and transported. Future work will focus on specifically diagnosing these issues with regards to model processes and emission estimates. There is current work in the GEOS-Chem community addressing the outflow of dust from Africa and quantifying background marine aerosol, but further work needs to be done in analyzing lofting mechanisms of aerosols over Europe and off of Asia along with removal processes in outflow regions. In particular, there is a need to investigate the possibility that pollutants are being rained out more quickly than observed.

CALIOP extinction profiles also provide a measure of aerosol type which we did not analyze here. It would be useful to examine differences in the profiles observed by CALIOP based on the inferred aerosol types (dust, marine, polluted). This would give us further insight into discrepancies in outflow regions, such as Asia, where dust, pollution, and marine aerosols are collocated.

Finally, the study of LRT is primarily motivated by a need to assess the downwind impact of pollutants at receptor sites. The use of surface based observations would aid in analyzing transported plumes as they are received and better to distinguish low altitude impacts that are less visible in satellite datasets. Here we only looked at surface data from two IMPROVE sites, which proved to be inconclusive. A goal of future work will be to include more ground based observations with increased temporal resolution, particularly more surface lidar data, such as from MPLNET and EARLINET as it becomes more readily available.

References

2010: The Air Quality Standards Regulations 2010. SI 2010/1001, TSO.

2010: National primary and secondary ambient air quality standards (NAAQS). Title 40 Code of Federal Regulations 50.

Akimoto, H., 2003: Global Air Quality and Pollution. *Science*, 302, 1716-1719.

Alexander, B., R. J. Park, D. J. Jacob, Q. B. Li, R. M. Yantosca, J. Savarino, C. C. W. Lee, and M. H. Thiemens, 2005: Sulfate formation in sea-salt aerosols: Constraints from oxygen isotopes. *Journal of Geophysical Research*, 110, 1-12.

Al-Saadi, J., J. Szykman, R. B. Pierce, C. Kittaka, D. Neil, D. A. Chu, L. Remer, L. Gumley, E. Prins, L. Weinstock, C. MacDonald, R. Wayland, F. Dimmick, and J. Fishman, 2005: Improving National Air Quality Forecasts with Satellite Aerosol Observations. *Bulletin of the American Meteorological Society*, 86, 1249-1261.

Ansmann, A., H. Baats, M. Tesche, D. Muller, D. Althausen, R. Engelmann, T. Pauliquevis, and P. Artaxo, 2009: Dust and smoke transport from Africa to South America: Lidat profiling over Cape Verde and the Amazon Rainforest. *Geophysical Research Letters*, 36.

Beer, R., T. A. Glavich, and D. M. Rider, 2001: Tropospheric emission spectrometer for the Earth Observing Systems Aura satellite. *Applied Optics* 40, 2356-2367.

Bell, M.L., J.M. Samet, F. Dominici, 2004: Time-series studies of particulate matter. *Annual Review of Public Health*, 25, 247-280.

Bell M.L., F. Dominici, J.M. Samet, 2005: A meta-analysis of time-series studies of ozone and mortality with comparison to the National Morbidity, Mortality, and Air Pollution Study. *Epidemiology*, 4, 436–445

Bell, M.L., R.D. Peng, and F. Dominci, 2006: The exposure–response curve for ozone and risk of mortality and the adequacy of current ozone regulations. *Environmental Health Perspectives*, 114:532-536.

Benkovitz, C., M. Scholtz, J. Pacyna, L. Tarrasón, J. Dignon, E. Voldner, P. Spiro, J. Logan, and T. Graedel, 1996: Global gridded inventories of anthropogenic emissions of sulfur and nitrogen. Journal of Geophysical Research, 101, 29239-29253.

Bond, T. C., D. G. Streets, K. F. Yarber, S. M. Nelson, J.-H. Woo, and Z. Klimont, 2004: A technology-based global inventory of black and organic carbon emissions from combustion. *Journal of Geophysical Research*, 109, 1-43.

Brock, C. A., P. K. Hudson, E. R. Lovejoy, A. Sullivan, J. B. Nowak, L. G. Huey, O. R. Cooper, D. J. Cziczo, J. d. Gouw, F. C. Fehsenfeld, J. S. Holloway, G. Hubler, B. G. Lafleur, D. M. Murphy, J. A. Neuman, D. K. N. Jr., D. A. Orsini, D. D. Parrish, T. B. Ryerson, D. J. Tanner, C. Warneke, R. J. Weber, and J. C. Wilson, 2004: Particle characteristics following cloud-modified transport from Asia to North America. *Journal of Geophysical Research*, 109, 1-17.

Burnett, R.T., J.R. Brook, W.T. Yung, R.E. Dales, and D. Krewski, 1997: Association between ozone and hospitalization for respiratory diseases in 16 Canadian cities. *Environmental Research*, 72: 24-31.

Chin, M., T. Diehl, P. Ginoux, and W. Malm, 2007: Intercontinental transport of pollution and dust aerosols: implications for regional air quality. *Atmospheric Chemistry and Physics*, 7, 5501-5517.

Chung, S. H. and J. H. Seinfeld, 2002: Global distribution and climate forcing of carbonaceous aerosols. *Journal of Geophysical Research*, 107, AAC 14-1-AAC 14-33.

Cooke, W., C. Liousse, H. Cachier, and J. Feichter, 1999: Construction of a 1 degree by 1 degree fossil fuel emission data set for carbonaceous aerosol and implementation and radiative impact in the ECHAM4 model. *Journal of Geophysical Research*, 104, 22137-22162.

Daniels, M.J., F. Dominici, J.M. Samet, S.L. Zeger, 2000: Estimating particulate matter-mortality dose-response curves and threshold levels: an analysis of daily time-series for the 20 largest US cities. *American Journal of Epidemiology*152, 397-406.

Deeter, M. N., L. K. Emmons, G. L. Francis, D. P. Edwards, J. C. Gille, J. X. Warner, B. Khattatov, D. Ziskin, J.-F. Lamarque, S.-P. Ho, V. Yudin, J.-L. Attie, D. Packman, J. Chen, D. Mao, J. R. Drummond, P. Novelli, and G. Sachse, 2004: Evaluation of operational radiances for the Measurements of Pollution in the Troposphere (MOPITT) instrument CO thermal band channels. *Journal of Geophysical Research*, 109, 1-12.

Deeter, M. N., D. P. Edwards, J. C. Gille, and J. R. Drummond, 2007: Sensitivity of MOPITT observations to carbon monoxide in the lower troposphere. *Journal of Geophysical Research*, 112, 1-9.

Derwent, R. G., D. S. Stevenson, W. J. Collins, and C. E. Johnson, 2004: Intercontinental transport and the origins of the ozone observed at surface sites in Europe. *Atmospheric Environment*, 38, 1891-1901.

Drury, E., D. J. Jacob, R. J. D. Spurr, J. Wang, Y. Shinozuka, B. E. Anderson, A. D. Clarke, J. Dibb, C. McNaughton, and R. Weber, 2010: Synthesis of satellite (MODIS), aircraft (ICARTT), and surface (IMPROVE, EPA-AQS, AERONET) aerosol observations over eastern North America to improve MODIS aerosol retrievals and constrain surface aerosol concentrations and sources. *Journal of Geophysical Research*, 115, D14204.

Drury, 2010: Synthesis of satellite (MODIS), aircraft (ICARTT), and surface (IMPROVE, EPA-AQS, AERONET) aerosol observations over eastern North America to improve MODIS aerosol retrievals and constrain surface aerosol concentrations and sources. *Journal of Geophysical Research*, 115, D14204.

Duncan, B. N. and I. Bey, 2004: A modeling study of the export pathways of pollution from Europe: Seasonal and interannual variations (1987-1997). *Journal of Geophysical Research*, 109, D08301.

Dunlea, E. J., P. F. DeCarlo, A. C. Aiken, J. R. Kimmel, R. E. Peltier, R. J. Weber, J. Tomlinson, D. R. Collins, Y. Shinozuka, C. S. McNaughton, S. G. Howell, A. D. Clarke, L. K. Emmons, E. C. Apel, G. G. Pfister, A. van Donkelaar, R. V. Martin, D. B. Millet, C. L. Heald, and J. L. Jimenez, 2009: Evolution of Asian aerosols during transpacific transport in INTEX-B. *Atmospheric Chemistry and Physics*, 9, 7257-7287.

Edwards, D. P., L. K. Emmons, D. A. Hauglustaine, D. A. Chu, J. C. Gille, Y. J. Kaufman, G. Pétron, L. N. Yurganov, L. Giglio, M. N. Deeter, V. Yudin, D. C. Ziskin, J. Warner, J.-F. Lamarque, G. L. Francis, S. P. Ho, D. Mao, J. Chen, E. I. Grechko, and J. R. Drummond, 2004: Observations of carbon monoxide and aerosols from the Terra satellite: Northern Hemisphere variability. *Journal of Geophysical Research*, 109, 1-17.

Evans, M. J. and D. J. Jacob, 2005: Impact of new laboratory studies of N 2 O 5 hydrolysis on global model budgets of tropospheric nitrogen oxides, ozone, and OH. *Geophysical Research Letters*, 32, 1-4.

Fairlie, D. T., D. J. Jacob, and R. J. Park, 2007: The impact of transpacific transport of mineral dust in the United States. *Atmospheric Environment*, 41, 1251-1266.

Fehsenfeld, F. C., G. Ancellet, T. S. Bates, A. H. Goldstein, R. M. Hardesty, R. Honrath, K. S. Law, A. C. Lewis, R. Leaitch, S. McKeen, J. Meagher, D. D. Parrish, A. A. P. Pszenny, P. B. Russell, H. Schlager, J. Seinfeld, R. Talbot, and R. Zbinden, 2006: International Consortium for Atmospheric Research on Transport and Transformation (ICARTT): North America to Europe: Overview of the 2004 summer field study. *Journal of Geophysical Research*, 111, 1-36.

Fiore, A. M., F. J. Dentener, O. Wild, C. Cuvelier, M. G. Schultz, P. Hess, C. Textor, M. Schulz, R. M. Doherty, L. W. Horowitz, I. A. MacKenzie, M. G. Sanderson, D. T. Shindell, D. S. Stevenson, S. Szopa, R. V. Dingenen, G. Zeng, C. Atherton, D. Bergmann, I. Bey, G. Carmichael, W. J. Collins, B. N. Duncan, G. Faluvegi, G. Folberth, M. Gauss, S. Gong, D. Hauglustaine, T. Holloway, I. S. A. Isaksen, D. J. Jacob, J. E. Jonson, J. W. Kaminski, T. J. Keating, A. Lupu, E. Marmer, V.

Montanaro, R. J. Park, G. Pitari, K. J. Pringle, J. A. Pyle, S. Schroeder, M. G. Vivanco, P. Wind, G. Wojcik, S. Wu, and A. Zuber, 2009: Multimodel estimates of intercontinental source-receptor relationships for ozone pollution. *Journal of Geophysical Research*, 114, 1-21.

Fuelberg, H. E., D. L. Harrigan, and W. Sessions, 2010: A meteorological overview of the ARCTAS 2008 mission. *Atmospheric Chemistry and Physics* 10, 26pp.

Generosa, S., I. Bey, M. Labonne, and F.-M. Breon, 2008: Aerosol vertical distribution in dust outflow over the Atlantic: Comparisons between GEOS-Chem and Cloud-Aerosol Lidar and Infrared Satellite Observation (CALIPSO). *Journal of Geophysical Research*, 113, 13pp.

Gent, J. F., E. W. Triche, T. R. Holford, K. Belanger, M. B. Bracken, W. S. Beckett, B. P. Leaderer, 2003: Association of low-level ozone and fine particles with respiratory symptoms in children with asthma. *Journal of the American Medical Association*, 290 (14):1859-1867.

Guenther, A., T. Karl, P. Harley, C. Wiedinmyer, P. I. Palmer, and C. Geron, 2006: Estimates of global terrestrial isoprene emissions using MEGAN (Model of Emissions of Gases and Aerosols from Nature). *Atmospheric Chemistry and Physics*, 6, 3181-3210.

Guerova, G., I. Bey, J. L. Attié, R. V. Martin, J. Cui, and M. Sprenger, 2006: Impact of transatlantic transport episodes on summertime ozone in Europe. *Atmospheric Chemistry and Physics*, 6, 2057-2072.

Heald, C. L., D. J. Jacob, D. B. A. Jones, P. I. Palmer, J. A. Logan, D. G. Streets, G. W. Sachse, J. C. Gille, R. N. Hoffman, and T. Nehrkorn, 2004: Comparative inverse

analysis of satellite (MOPITT) and aircraft (TRACE-P) observations to estimate Asian sources of carbon monoxide. *Journal of Geophysical Research*, 109, 1-17.

Heald, C. L., D. J. Jacob, R. J. Park, B. Alexander, T. D. Fairlie, R. M. Yantosca, and D. A. Chu, 2006: Transpacific transport of Asian anthropogenic aerosols and its impact on surface air quality in the United States. *Journal of Geophysical Research*, 111, 1-13.

Hudman, R. C., D. J. Jacob, O. R. Cooper, M. J. Evans, C. L. Heald, R. J. Park, F. Fehsenfeld, F. Flocke, J. Holloway, G. Hubler, K. Kita, M. Koike, Y. Kondo, A. Neuman, J. Nowak, S. Oltmans, D. Parrish, J. M. Roberts, and T. Ryerson, 2004: Ozone production in transpacific Asian pollution plumes and implications for ozone air quality in California. *Journal of Geophysical Research*, 109, 1-14.

Hudman, R. C., D. J. Jacob, S. Turquety, E. M. Leibensperger, L. T. Murray, S. Wu, A. B. Gilliland, M. Avery, T. H. Bertram, W. Brune, R. C. Cohen, J. E. Dibb, F. M. Flocke, A. Fried, J. Holloway, J. A. Neuman, R. Orville, A. Perring, X. Ren, G. W. Sachse, H. B. Singh, A. Swanson, and P. J. Wooldridge, 2007: Surface and lightning sources of nitrogen oxides over the United States: Magnitudes, chemical evolution, and outflow. *Journal of Geophysical Research*, 112, 1-14.

Hunt, W. H., D. M. Winker, M. A. Vaughan, K. A. Powell, P. L. Lucker, and C. Weimer, 2009: CALIPSO Lidar Description and Performance Assessment. *Journal of Atmospheric and Oceanic Technology*, 26, 1214-1228.

Jaffe, D., T. Anderson, D. Covert, R. Kotchenruther, B. Trost, J. Danielson, W. Simpson, T. Berntsen, S. Karlsdottir, D. Blake, J. Harris, G. Carmichael, and I. Uno, 1999:

Transport of Asian Air Pollution to North America. *Geophysical Research Letters*, 26, 711-714.

Kaufman, Y., D. Tanreacute;, L. Remer, E. Vermote, A. Chu, and B. Holben, 1997: Operational remote sensing of tropospheric aerosol over land from EOS moderate resolution imaging spectroradiometer. *Journal of Geophysical Research*, 102, 17051-17067.

Keating, T. J. and A. Zuber, 2007: Hemispheric Transport of Air Pollution 2007.

Kittaka, C., D. M. Winker, M. A. Vaughan, A. Omar, and L. A. Remer: Intercomparison of CALIOP and MODIS aerosol optical depth retrievals. *Atmos. Meas. Tech. Discuss.*, 3, 3319-3344.

Kopacz, M., D. J. Jacob, J. A. Fisher, J. A. Logan, L. Zhang, I. A. Megretskaia, R. M. Yantosca, K. Singh, D. K. Henze, J. P. Burrows, M. Buchwitz, I. Khlystova, W. W. McMillan, J. C. Gille, D. P. Edwards, A. Eldering, V. Thouret, and P. Nedelec, 2010: Global estimates of CO sources with high resolution by adjoint inversion of multiple satellite datasets (MOPITT, AIRS, SCIAMACHY, TES). *Atmospheric Chemistry and Physics*, 10, 855-876.

Kuhns, H., M. Green, and V. Etyemezian, 2003: Big Bend Regional Aerosol and Visibility Observational (BRAVO) Study Emissions Inventory. Report prepared for BRAVO Steering Committee.

Kulmala, M., A. Reissell, M. Sipilä, B. Bonn, T. M. Ruuskanen, K. E. J. Lehtinen, V.-M. Kerminen, and J. Ström, 2006: Deep convective clouds as aerosol production engines: Role of insoluble organics. *Journal of Geophysical Research*, 111, D17202.

Lapina, K., 2010: Marine organic aerosol. Personal communication to B. Ford. August 2010.

Levy, H. I., 1974: Photochemistry of the Troposphere. Advances in Photochemistry, J. N. Pitts, G. S. Hammond, and K. Gollnick, Eds., John Wiley & Sons, 369-524.

Levy, H. I. and W. J. Moxim, 1989: Simulated global distribution and depocition of reactive nitrogen emitted by fossil fuel combustion. *Tellus B*, 41, 256-271.

Levy, R. C., L. A. Remer, J. V. Martins, Y. J. Kaufman, A. Plana-Fattori, J. Redemann, and B. Wenny, 2005: Evaluation of the MODIS Aerosol Retrievals over Ocean and Land during CLAMS. *Journal of the Atmospheric Sciences*, 62, 974-992.

Li, Q., D. J. Jacob, I. Bey, P. I. Palmer, B. N. Duncan, B. D. Field, R. V. Martin, A. M. Fiore, R. M. Yantosca, D. D. Parrish, P. G. Simmonds, and S. J. Oltmans, 2002: Transatlantic transport of pollution and its effects on surface ozone in Europe and North America. *Journal of Geophysical Research*, 107.

Li, Q., D. J. Jacob, R. Park, Y. Wang, C. L. Heald, R. Hudman, R. M. Yantosca, R. V. Martin, and M. Evans, 2005: North American pollution outflow and the trapping of convectively lifted pollution by upper-level anticyclone. *Journal of Geophysical Research*, 110, 1-18.

Liao, H., D. K. Henze, J. H. Seinfeld, S. Wu, and L. J. Mickley, 2007: Biogenic secondary organic aerosol over the United States: Comparison of climatological simulations with observations. *Journal of Geophysical Research*, 112, 1-19.

Lin, J.-T., D. Youn, X.-Z. Liang, and D. J. Wuebbles, 2008: Gobal model simulation of summertime ozone diurnal cycle and its sensititvity to PBL mixing, spatial resolution, and emissions. *Atmospheric Environment*, 42, 14.

Lin, J.-T. and M. B. McElroy, 2010: Impacts of boundary layer mixing on pollutant vertical profiles in the lower troposphere: Implications to satellite remote sensing. *Atmospheric Environment*, 44, 14.

Lin, S. X. Liu, L.H. Le, and S-A. Hwang, 2008: Chronic exposure to ambient ozone and asthma hospital admissions among children. *Environmental Health Perspectives*, 116(12), 1725-1730.

Liu, H., D. Jacob, I. Bey, and R. Yantosca, 2001: Constraints from 210 Pb and 7 Be on wet deposition and transport in a global three-dimensional chemical tracer model driven by assimilated meteorological fields. *Journal of Geophysical Research*, 106, 12109-12128.

Liu, H., D. J. Jacob, I. Bey, R. M. Yantosca, and B. N. Duncan, 2003: Transport pathways for Asian pollution outflow over the Pacific: Interannual and seasonal variations. *Journal of Geophysical Research*, 108, 18pp.

Liu, J., D. L. Mauzerall, L. W. Horowitz, P. Ginoux, and A. M. Fiore, 2009a: Evaluating inter-continental transport of fine aerosols: (1) Methodology, global aerosol distribution and optical depth. *Atmospheric Environment*, 43, 4327-4338.

Liu, J., D.L. Mauzerall, and L.W. Horowitz, 2009b: Evaluating inter-continental transport of fine aerosols: (2) Global health impact. *Atmospheric Environment*, 43, 4339-4347.

Liu, Z., M. A. Vaughan, D. M. Winker, C. A. Hostetler, L. R. Poole, D. Hlavka, W. Hart, and M. McGill, 2004: Use of probability distribution functions for discriminating between cloud and aerosol in lidar backscatter data. *Journal of Geophysical Research*, 109, 1-13.

Luo, M., C. P. Rinsland, C. D. Rodgers, J. A. Logan, H. Worden, S. Kulawik, A. Eldering, A. Goldman, M. W. Shephard, M. Gunson, and M. Lampel, 2007: Comparison of carbon monoxide measurements by TES and MOPITT: Influence of a priori data and instrument characteristics on nadir atmospheric species retrievals. Journal *of Geophysical Research*, 112, 1-13.

Malm, W., J. Sisler, D. Huffman, R. Eldred, and T. Cahill, 1994: Spatial and seasonal trends in particle concentration and optical extinction in the United States. *Journal of Geophysical Research*, 99, 1347-1370.

Martin, R. V., D. J. Jacob, R. M. Yantosca, M. Chin, and P. Ginoux, 2003: Global and regional decreases in tropospheric oxidants from photochemical effects of aerosols. *Journal of Geophysical Research*, 108, 14pp.

Matsuki, A., Y. Iwasaka, K. Osada, K. Matsunaga, M. Kido, Y. Inomata, D. Trochkine, C. Nishita, T. Nezuka, T. Sakai, D. Zhang, and S.-A. Kwon, 2003: Seasonal dependence of the long-range transport and vertical distribution of free tropospheric aerosols over east Asia: On the basis of aircraft and lidar measurements and isentropic trajectory analysis. *Journal of Geophysical Research*, 108, 8663.

Olivier, J. G. J. and J. J. M. Berdowski, 2001: Global emissions sources and sinks. The Climate System, J. Berdowski, R. Guicherit, and B. J. Heij, Eds., A.A. Balkema Publishers/Swets & Zeitlinger Publishers, 33-78.

Olivier, J. G. J., J. J. M. Berdowski, J. A. H. W. Peters, J. Bakker, A. J. H. Visschedijk, and J.-P. J. Bloos, 2001: Applications of EDGAR. Including a description of EDGAR 3.0: reference database with trend data for 1970-1995, 142 pp.

Osterman, G., ed., 2007: Tropospheric Emission Spectrometer (TES) Validation Report Version F04_04 Data.

Owen, R. C., O. R. Cooper, A. Stohl, and R. E. Honrath, 2006: An analysis of the mechanisms of North American pollutant transport to the central North Atlantic lower free troposphere. *Journal of Geophysical Research*, 111, 1-14.

Park, R. J., D. J. Jacob, M. Chin, and R. V. Martin, 2003: Sources of carbonaceous aerosols over the United States and implications for natural visibility. *Journal of Geophysical Research*, 108, AAC 5-1 - AAC 5-14.

Park, R. J., D. J. Jacob, B. D. Field, R. M. Yantosca, and M. Chin, 2004: Natural and transboundary pollution influences on sulfate-nitrate-ammonium aerosols in the United States: Implications for policy. *Journal of Geophysical Research,* 109, 1-17.

Parrington, M., D. B. A. Jones, K. W. Bowman, L. W. Horowitz, A. M. Thompson, D. W. Tarasick, and J. C. Witte, 2008: Estimating the summertime tropospheric ozone distribution over North America through assimilation of observations from the Tropospheric Emission Spectrometer. *Journal of Geophysical Research,* 113, 1-18.

Parrish, D. D., D. T. Allen, T. S. Bates, M. Estes, F. C. Fehsenfeld, G. Feingold, R. Ferrare, R. M. Hardesty, J. F. Meagher, J. W. Nielsen-Gammon, R. B. Pierce, T. B. Ryerson, J. H. Seinfeld, and E. J. Williams, 2009: Overview of the Second Texas Air Quality Study (TexAQS II) and the Gulf of Mexico Atmospheric Composition and Climate Study (GoMACCS). *Journal of Geophysical Research,* 114, 1-28.

Perry, K. D., T. A. Cahill, R. C. Schnell, and J. M. Harris, 1999: Long-range transport of anthropogenic aerosols to the National Oceanic and Atmospheric Administration baseline station at Mauna Loa Observatory, Hawaii. *Journal of Geophysical Research*, 104, 18521-18534.

Pope, C.A., 2000. Invited commentary: particulate matter-mortality exposure response relations and threshold. *American Journal of Epidemiology*, 152, 407-412.

Pope, C.A., R.T. Burnett, M.J. Thun, E.E. Calle, D. Krewski, K. Ito and G.D. Thurston, 2002: Lung cancer, cardiopulmonary mortality, and long-term exposure to fine particulate air pollution, *JAMA*, 287, 1132–1141.

Pope, C., R. Burnett, G. Thurston, M. Thun, E. Calle, D. Krewski and J. Godleski, 2004: Cardiovascular mortality and long-term exposure to particulate air pollution – epidemiological evidence of general pathophysiological pathways of disease, *Circulation*, 109, 71–77.

Pope, C.A. and D.W. Dockery, 2006: Health effects of fine particulate air pollution: lines that connect. *Journal of Air and Waste Management Association*, 56, 709–742.

Price, H. U., D. A. Jaffe, O. R. Cooper, and P. V. Doskey, 2004: Photochemistry, ozone production, and dilution during long-range transport episodes from Eurasia to the northwest United States. *Journal of Geophysical Research*, 109, 1-10.

Prospero, J., 1981: Aeolian transport to the world ocean. . The Oceanic Lithosphere, C. Emiliani, Ed., Wiley, 801-874.

Prospero, 1999: Long-term measurements of the transport of African mineral dust to the southeastern United States: Implications for regional air quality. *Journal of Geophysical Research*, 104, 15917-15927.

Qing, L., L. Jaegle, D. A. Jaffe, P. Weiss-Penzias, A. Heckman, and J. A. Snow, 2004: Long-range transport of Asia pollution to the northeast Pacific: Seasonal variations and transport pathways of carbon monoxide. *Journal of Geophysical Research*, 109, 16pp.

Quinn, P. K., G. Shaw, E. Andrews, E. G. Dutton, T. Ruoho-Airola, and S. L. Gong, 2007: Arctic haze: current trends and knowledge gaps. *Tellus B*, 59, 99-114.

Rasch, P. J., M. C. Barth, and J. T. Kiehl, 2000: A description of the global sulfur cycle and its controlling processes in the National Center for Atmospheric Research Community Climate Model, Version 3. *Journal of Geophysical Research*, 105, 19pp.

Reidmiller, D. R., D. A. Jaffe, D. Chand, S. Strode, P. Swartzendruber, G. M. Wolfe, and J. A. Thornton, 2009: Interannual variability of long-range transport as seen at the Mt. Bachelor observatory. Atmospheric Chemistry and Physics, 9, 557-572.

Remer, L. A., Y. J. Kaufman, D. Tanré, S. Mattoo, D. A. Chu, J. V. Martins, R. R. Li, C. Ichoku, R. C. Levy, R. G. Kleidman, T. F. Eck, E. Vermote, and B. N. Holben, 2005: The MODIS Aerosol Algorithm, Products, and Validation. *Journal of the Atmospheric Sciences*, 62, 947-973.

Rodgers, C. D., 2000: Inverse Methods for Atmospheric Sounding: Theory and Practice. Series on Atmospheric, Oceanic, and Planetary Physics, World Scientific Publishing Co., 240 pp.

Schultz, M. G. and I. Bey, 2004: Numerical modeling of long-range pollution transport. *Intercontinental transport of air pollution*, A. Stohl, Ed., Springer-Verlag, 197-223.

Singh, H. B., W. H. Brune, J. H. Crawford, D. J. Jacob, and P. B. Russell, 2006: Overview of the summer 2004 Intercontinental Chemical Transport Experiment-North America (INTEX-A). *Journal of Geophysical Research*, 111, 1-17.

Stohl, A., S. Eckhardt, C. Forster, P. James, and N. Spichtinger, 2002: On the pathways and timescales of intercontinental air pollution transport. *Journal of Geophysical Research*, 107, 6-17.

van der Werf, G. R., J. T. Randerson, L. Giglio, G. J. Collatz, P. S. Kasibhatla, and A. F. Arellano Jr, 2006: Interannual variability in global biomass burning emissions from 1997 to 2004. *Atmospheric Chemistry and Physics*, 6, 3423-3441.

van Donkelaar, A., R. V. Martin, M. Brauer, R. Kahn, R. Levy, C. Verduzco, and P. J. Villeneuve, 2010: Global Estimates of Ambient Fine Particulate Matter Concentrations from Satellite-Based Aerosol Optical Depth: Development and Application. Environ Health Perspect, 118.

Vestreng, V., K. Mareckova, S. Kakareka, A. Malchykhina, and T. Kukharchyk, 2007: Inventory Review 2007; Emission Data reported to LRTAP Convention and NEC Directive, MSC-W Technical Report 1/07.

Wesely, M. L., 1989: Parameterization of surface resistances to gaseous dry deposition in regional-scale numerical models. *Atmospheric Environment*, 23, 1293-1304.

Winker, D. M., J. R. Pelon, and M. P. McCormick, 2003: The CALIPSO mission: spaceborne lidar for observation of aerosols and clouds. Lidar Remote Sensing for Industry and Environment Monitoring III, Hangzhou, China, SPIE, 1-11.

Winker, D. M., J. Pelon, J. A. Coakley, S. A. Ackerman, R. J. Charlson, P. R. Colarco, P. Flamant, Q. Fu, R. M. Hoff, C. Kittaka, T. L. Kubar, H. Le Treut, M. P.

McCormick, G. Mégie, L. Poole, K. Powell, C. Trepte, M. A. Vaughan, and B. A. Wielicki, 2010: The CALIPSO Mission: A Global 3D View of Aerosols and Clouds. *Bulletin of the American Meteorological Society*, 91, 1211-1229.

Yevich, R. and J. A. Logan, 2003: An assessment of biofuel use and burning of agricultural waste in the developing world. *Global Biogeochemical Cycles*, 17, 1095, 44pp.

Yu, H., L. A. Remer, M. Chin, H. Bian, R. G. Kleidman, and T. Diehl, 2008: A satellite-based assessment of transpacific transport of pollution aerosol. *Journal of Geophysical Research*, 113, 1-15.

Yu, H., M. Chin, D. M. Winker, A. H. Omar, Z. Liu, C. Kittaka, and T. Diehl, 2010: Global view of aerosol vertical distributions from CALIPSO lidar measurements and GOCART simulations: Regional and seasonal variations. Journal of Geophysical Research, 115, D00H30.

Zhang, J. and J. S. Reid, 2006: MODIS aerosol product analysis for data assimilation: Assessment of over-ocean level 2 aerosol optical thickness retrievals. Journal of Geophysical Research, 111, 1-17.

Zhang, Q., D. G. Streets, G. R. Carmichael, K. B. He, H. Huo, A. Kannari, Z. Klimont, I. S. Park, S. Reddy, J. S. Fu, D. Chen, L. Duan, Y. Lei, L. T. Wang, and Z. L. Yao, 2009: Asian emissions in 2006 for the NASA INTEX-B mission. Atmospheric Chemistry and Physics, 9, 5131-5153.